iScience

CellPress

Article

Dynamic Interaction of USP14 with the Chaperone HSC70 Mediates Crosstalk between the Proteasome, ER Signaling, and Autophagy

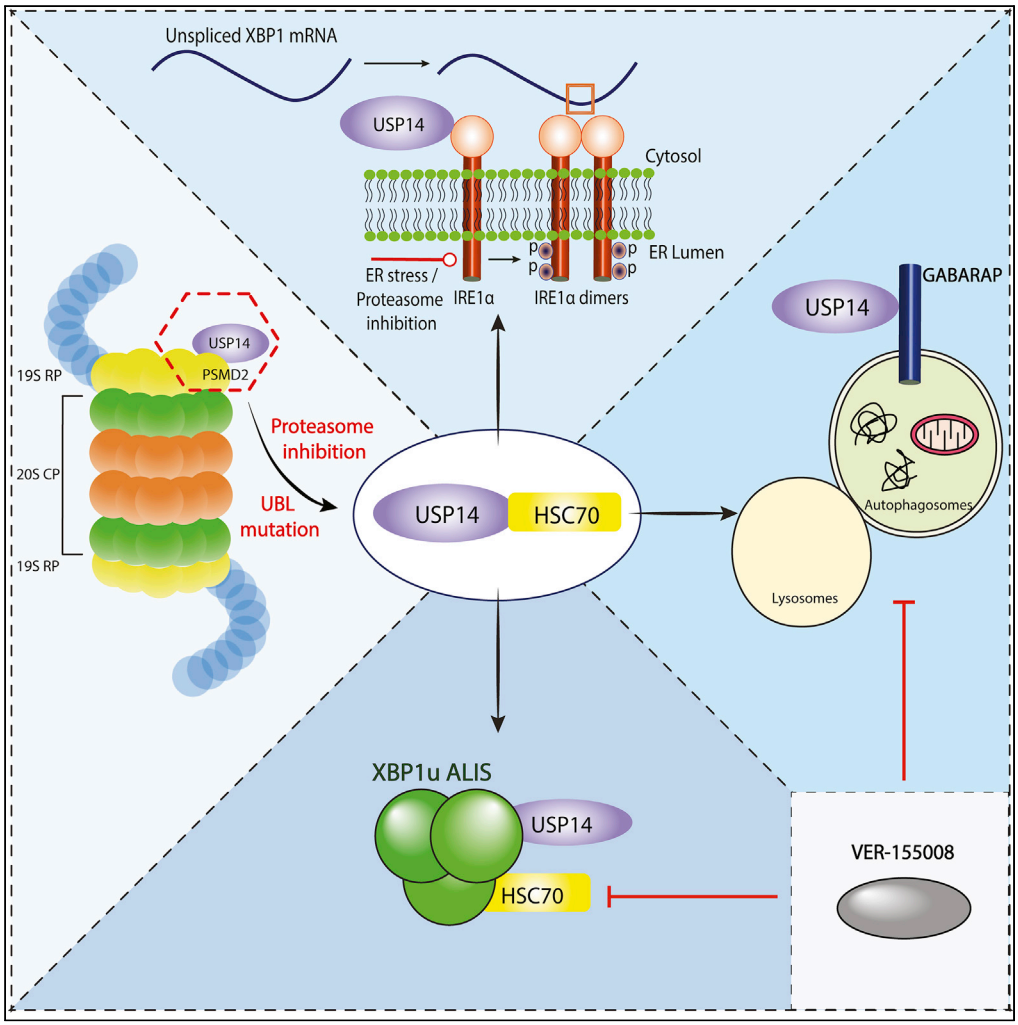

Vignesh Srinivasan, Celine Bruelle, Enzo Scifo, Dan Duc Pham, Rabah Soliymani, Maciej Lalowski, Dan Lindholm

dan.lindholm@helsinki.fi

HIGHLIGHTS

USP14 binds HSC70 upon proteasome inhibition

This rises GABARAP autophagosomes in HD

Srinivasan et al., iScience *23*, 100790
January 24, 2020
https://doi.org/10.1016/j.isci.2019.100790

iScience

CellPress

Article

Dynamic Interaction of USP14 with the Chaperone HSC70 Mediates Crosstalk between the Proteasome, ER Signaling, and Autophagy

Vignesh Srinivasan,[1,2] Celine Bruelle,[1,2] Enzo Scifo,[1,4] Dan Duc Pham,[1,2] Rabah Soliymani,[1,3] Maciej Lalowski,[1,3] and Dan Lindholm[1,2,5,*]

SUMMARY

USP14 is a deubiquitinating enzyme associated with the proteasome important for protein degradation. Here we show that upon proteasome inhibition or expression of the mutant W58A-USP14, association of USP14 with the 19S regulatory particle is disrupted. MS-based interactomics revealed an interaction of USP14 with the chaperone, HSC70, in neuroblastoma cells. Proteasome inhibition enhanced binding of USP14 to HSC70, and to XBP1u and IRE1α proteins, demonstrating a role in the unfolded protein response. Striatal neurons expressing mutant huntingtin exhibited reduced USP14 and HSC70 levels, whereas inhibition of HSC70 downregulated USP14. Furthermore, proteasome inhibition or use of the mutant W58A-USP14 facilitated the interaction of USP14 with the autophagy protein, GABARAP. Functionally, overexpression of W58A-USP14 increased GABARAP positive autophagosomes in striatal neurons, and this was abrogated using the HSC70 inhibitor, VER-155008. Modulation of the USP14-HSC70 axis may represent a potential therapeutic target in HD to beneficially influence multiple proteostasis pathways.

INTRODUCTION

USP14 is a deubiquitinating enzyme (DUB) involved in degradation of protein substrates by cleavage and trimming of ubiquitin chains at the proteasome (Kim and Goldberg, 2017). USP14 is highly expressed in the nervous system and its deficiency leads to progressive neurological dysfunctions including ataxia and muscle paralysis (Lappe-Siefke et al., 2009). Loss of USP14 is associated with defective ubiquitin recycling and deficiency in free ubiquitin (Chen et al., 2009). Studies in different cancer cells have revealed a role of USP14 in the degradation of specific protein substrates as shown by the use of chemical blockers (Cai et al., 2017; Ding et al., 2018). The underlying mechanisms for the various actions of USP14 are not fully understood. USP14 is a *bona fide* proteasome-bound protein, but recent studies have established a proteasome-independent role of USP14 in the regulation of autophagy in cells (Xu et al., 2016) and in c-jun N-terminal kinase signaling at the neuromuscular junction (Vaden et al., 2015). Previous studies have further shown that USP14 can interact with inositol-requiring enzyme 1α (IRE1α) on the ER membrane and inhibit ER-associated protein degradation (Nagai et al., 2009). We recently observed that USP14 is cytoprotective in neuronal cells by reducing protein aggregates, as observed in models of Huntington disease (HD) (Hyrskyluoto et al., 2014). Part of this effect evoked by USP14 was ascribed to the ubiquitin proteasome system (UPS) and to the counteraction of IRE1α-mediated ER stress signaling. However, the precise mechanisms underlying the different cellular roles of USP14 and in the pathology of various diseases are not fully understood.

In the present work, we have used a proteomic approach to search for interacting partners of USP14 in the context of neuronal cells. To study the complementary roles of USP14 in a proteasome-free context, we constructed UBL domain mutant USP14 with a reduced ability to bind to PSMD2/RPN1 in the proteasome 19S regulatory particle (RP). We subsequently utilized inhibitors of proteasome causing dissociation of USP14 from PSMD2, a component of the proteasome 19S RP. Upon proteasome inhibition, USP14 interacted with HSC70/HSPA8 in neuronal cells, whereas the UBL mutant, W58A-USP14, bound the chaperone avidly even without proteasome blockage. The small molecule compound, VER-155008, that inhibits HSC70 affected the levels of USP14 in cells, and the interaction of USP14 with HSC70 reciprocally regulated their protein levels. Furthermore, we showed that USP14 can interact with other proteins in the cell, including unspliced X-box binding protein-1 that forms aggresome-like induced structures (called ALIS) in the neuronal cells following proteasome inhibition. These structures were sensitive to HSC70 inhibition by VER-155008 and the levels of USP14, as shown in neuroblastoma cell lines after downregulation of USP14 using shRNA. In mutant huntingtin (Htt)-expressing striatal cells with reduced

[1]Medicum, Department of Biochemistry and Developmental Biology, Faculty of MedicineUniversity of Helsinki, P.O. Box 63, FIN-00014 Helsinki, Finland

[2]Minerva Foundation Institute for Medical Research, Biomedicum Helsinki 2U, Tukholmankatu 8, FIN-00290 Helsinki, Finland

[3]Meilahti Clinical Proteomics Core Facility HiLIFE, University of Helsinki, Helsinki, Finland

[4]Molecular and Cellular Cognition Lab, German Center for Neurodegenerative Diseases, Venusberg-Campus 1, Building 99, 53127 Bonn, Germany

[5]Lead Contact

*Correspondence: dan.lindholm@helsinki.fi

https://doi.org/10.1016/j.isci.2019.100790

USP14 levels, the XBP1u positive ALIS also decreased. As reported earlier, USP14 also interacted with the ER signaling protein, IRE1α, affecting its phosphorylation status and endonuclease splicing activity albeit differentially upon proteasome inhibition. Most significantly, USP14 interacted with the autophagy-linked protein gamma-aminobutyric acid receptor-associated protein (GABARAP) involved in the late stage of autophagy (Weidberg et al., 2010b). We observed that the UBL mutant, W58A-USP14 promoted the formation of GABARAP-positive autophagosomal structures in striatal neuronal cells, a process that was reduced by the HSC70 inhibitor, VER-155008. Together these data demonstrate that USP14 and its interaction with HSC70 affect autophagy and other cellular processes in neuronal cells.

RESULTS

USP14 Interacts with the Proteasome 19S Subunit PSMD2 via the UBL Domain

USP14 is an important proteasome-associated DUB that removes ubiquitin chains from protein substrates destined for degradation. However, USP14 may also have non-proteasomal functions by binding to specific proteins in the cell as shown for the IRE1α in the ER membrane (Hyrskyluoto et al., 2014; Nagai et al., 2009). The mechanisms and factors governing the de-attachment of USP14 from the proteasome are not fully understood. We observed that lactacystin (a chemical compound that inhibits the proteasome) caused release of USP14 from PSMD2 in the proteasome 19S RP in SH-SY5Y human neuroblastoma cells (Figure 1A). To study the structural requirement for USP14 binding to the proteasome 19S subunit, we focused on the amino-terminal ubiquitin-like domain (UBL) with a stretch of amino acids 54-60 that is conserved between species (Figure 1B). Amino acid 58 (tryptophan, W) in the UBL domain was subsequently mutated to alanine (A) to generate the USP14 mutant construct, W58A-USP14 (Figure 1C). Immunoprecipitation experiments in SH-SY5Y neuroblastoma cells using the Flag-tagged USP14 constructs revealed that wild-type USP14 avidly interacted with the protein PSMD2/RPN1 of the proteasome 19S RP, whereas the UBL-mutant W58A-USP14 construct did not (Figure 1D). In order to investigate the catalytic activity of the generated mutant, we employed the ubiquitin-vinyl methyl ester (Ub-VME) substrate assay (Borodovsky et al., 2002). The mutant USP14 construct showed no significant deubiquitinating activity in this assay performed with mouse neuroblastoma cells (Figure 1E). In contrast, wild-type USP14 was active as indicated by the presence of an additional band corresponding to the Ub-VME substrate bound to the catalytic site of USP14 (Figure 1E, arrow). These results show that amino acid 58 in the UBL region is vital for the interaction of USP14 with the PSMD2/RPN1 in the proteasome 19S RP.

Identification of HSC70 as Interacting Partner of USP14

In order to identify USP14 interacting partners, we designed a proteomics strategy using a novel mammalian retroviral-based expression vector pES-NTAP-Puro (a modified version of pCeMM-NTAP(SG)-Gw vector, EURO-SCARF) (see Transparent Methods). We generated USP14-NTAP-Puro stably expressing SH-SY5Y cell lines and employed tandem affinity purification (TAP) (Burckstummer et al., 2006) followed by tandem MS sequencing, bioinformatic analysis, and functional validation of selected interacting partners for USP14 (Figure S2) (Scifo et al., 2013, 2015). The details of NTAP-puro construction, in which the IRES-GFP cassette has been replaced with IRES-Puro, allowing selection on puromycin are shown in Figure S1. The functionality of pES-NTAP-Puro was verified by cloning and expression of human USP14 in SH-SY5Y cells. Following SAINT filtering, we identified in total 26 USP14 IP, 23 of which form the 26S proteasomal assembly (Figure 2A). A list of the USP14 IP, isolated from SH-SY5Y USP14-NTAP-Puro stable cells, is shown in Table S1. Nineteen (73%) USP14 high-confidence IP (HCIP) were previously determined by a variety of methods including affinity-capture MS, affinity-capture Western, or co-fractionation (Biogrid/homo-sapiens/usp14). In addition, we identified HSPA8/HSC70, heat shock 71 kDa protein 8 as an interactor of USP14 (Figure 2A and Table S1). In order to functionally validate the interaction of USP14 with HSC70, SH-SY5Y cells stably expressing Flag-HA-GFP and Flag-HA-WT-USP14 were generated. The cells were lysed and protein levels of HSC70 analyzed using immunoblotting. Stable expression of WT-USP14 increased the protein levels of HSC70 (Figure 2B). Furthermore, transient overexpression of WT-USP14 in neuroblastoma cells also increased HSC70 protein levels, and this effect was more pronounced for the W58A-USP14 mutant (Figure 2C). These results indicate that the interaction of USP14 with HSC70 increases the protein levels of the latter probably affecting its multiple cellular functions.

Inhibition of Proteasome Affects the Interaction of USP14 with HSC70

To validate our findings on HSC70, we carried out co-immunoprecipitation experiments using the W58A-USP14 mutant, transiently expressed in SH-SY5Y cells. In these experiments, the mutant W58A-USP14 readily interacted with HSC70, whereas, WT-USP14 exhibited less ability to bind to the chaperone (Figure 2D). To investigate

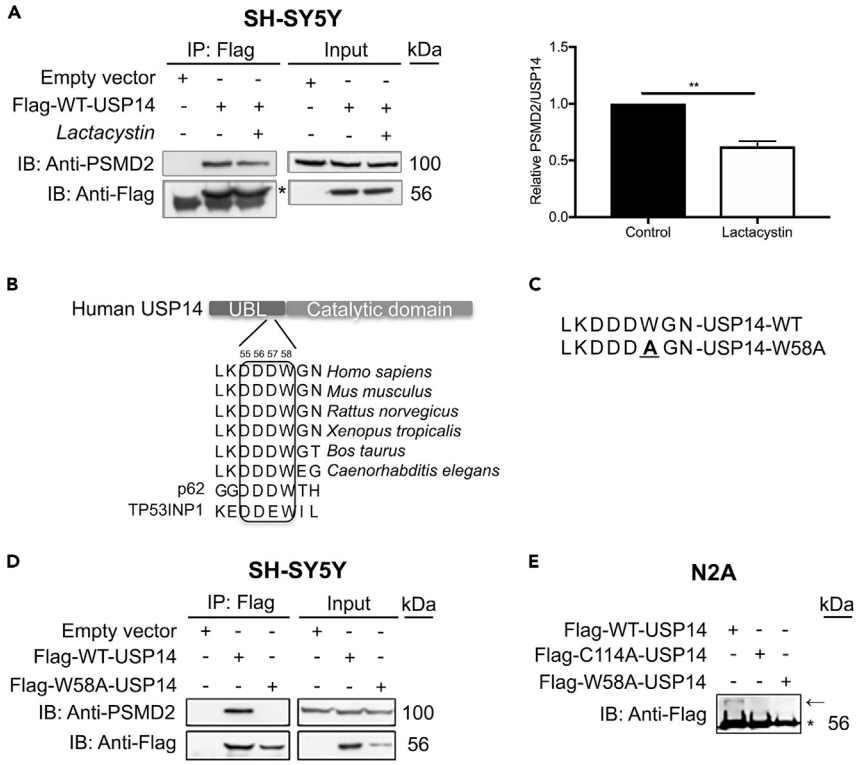

Figure 1. Proteasome Inhibition Disrupts the Association of USP14 with PSMD2 in the Proteasome 19S Subunit

(A) SH-SY5Y cells overexpressing Flag-WT-USP14 were treated with DMSO or lactacystin (5 μM, 6 h) and subjected to immunoprecipitation. The complexes were analyzed by immunoblotting for PSMD2 of the proteasome 19S regulatory particle and Flag. Densitometry ratio of the PSMD2-USP14 interaction is presented in the right panel.

(B) Protein sequence of USP14 UBL domain is conserved among species.

(C) Tryptophan (W) mutated to alanine (A) in W58A-USP14 sequence is underlined.

(D) Immunoprecipitation of Flag-WT-USP14 or Flag-W58A-USP14 constructs with Flag antibody and analyzed by immunoblotting for PSMD2 and Flag.

(E) Cell lysates of Neuro2A cell overexpressing Flag-WT-USP14, Flag-C114A-USP14, or Flag-W58A-USP14 were incubated with the Ub-VME substrate for 3 h to assess DUB activity. The mixture was analyzed by immunoblotting for Flag, to detect the substrate-bound DUBs (shows as an additional band on the IB, marked by an arrow; star marks the overexpressed Flag constructs).

Abbreviations: USP14, ubiquitin-specific protease-14; WT, wild-type; PSMD2, 26S proteasome regulatory subunit 2; UBL, ubiquitin-like; Ub-VME, ubiquitin-vinyl methyl ester; DUB, deubiquitinating enzyme; IB, immunoblotting; IP, immunoprecipitation. (A) n = 3, **- $p \leq 0.01$ Student's t-test.

whether the association of WT-USP14 with HSC70 may require some additional stimulus, we used bortezomib to inhibit the proteasome (Figure 2E). Upon proteasome inhibition, the association of USP14 with HSC70 was clearly increased (Figure 2E, lane 3). This is likely related to the fact that inhibition of the proteasome liberates more USP14 from its binding to PSMD2 in the proteasome 19S RP (Figure 1). Thus, our findings indicate that proteasome inhibition induced an increase in association of WT-USP14 with HSC70. To further corroborate the interaction of USP14 and HSC70, we overexpressed Flag-USP14 constructs in conjunction with GFP-WT-HSC70 in SH-SY5Y cells followed by immunoprecipitations. The resulting IP complexes were analyzed by immunoblotting with anti-Flag and anti-GFP antibodies. GFP-WT-HSC70 co-immunoprecipitated with Flag-WT-USP14 and the interaction was increased in the presence of MG132 (Figure 2F). Mutant W58A-USP14 exhibited a high inherent ability to associate with HSC70, exceeding that observed with WT-USP14 after proteasome inhibition (Figure 2F). Together these results show that the interaction of USP14 with HSC70 in neuroblastoma cells is sensitive to proteasome inhibition.

USP14 Interacts with XBP1u Protein upon Proteasome Inhibition

We and others have previously shown that USP14 can bind to the ER(ER)-resident kinase, IRE1α, affecting its phosphorylation status in models of HD (Hyrskyluoto et al., 2014). Activation of IRE1α mediates various

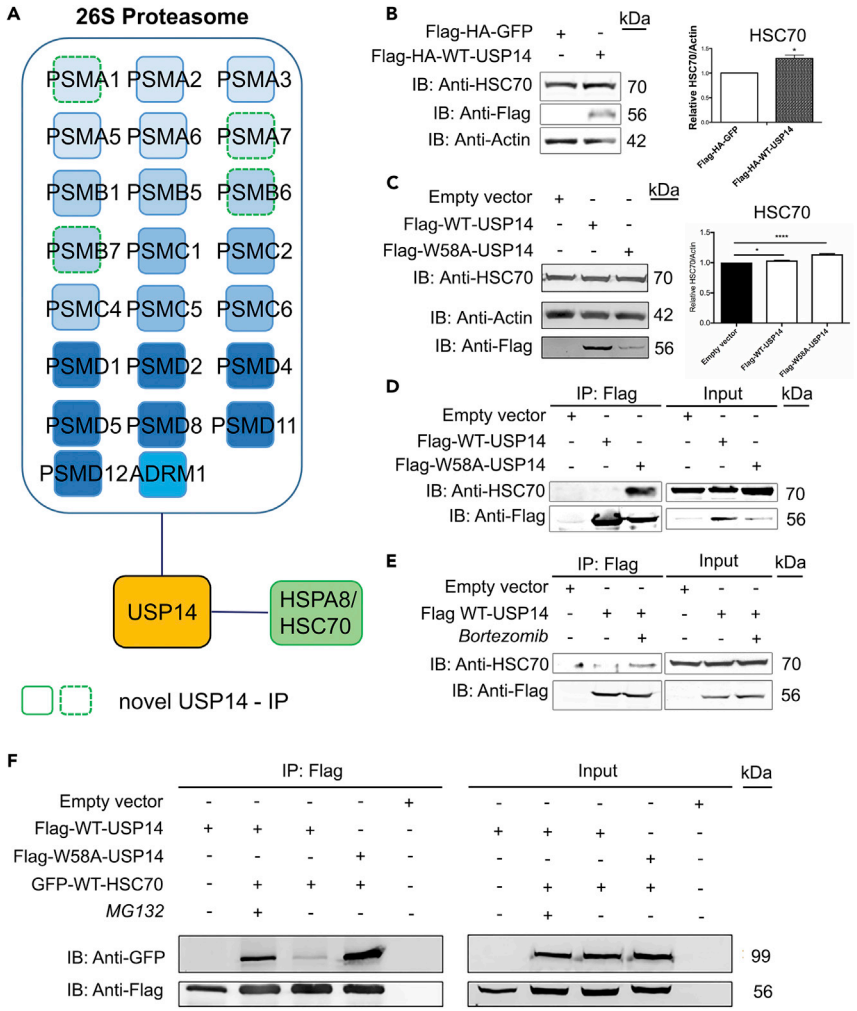

Figure 2. Proteasome Inhibition or Expression of Mutant W58A-USP14 Enhances the Association of USP14 with HSC70

Affinity purification and bioinformatic analysis of USP14-interacting partners were performed as depicted in Figure S2.

(A) The identified USP14-interacting partners are depicted figuratively where most of the hits constitute the 26S proteasome complex and have previously been reported. The interaction of USP14 with HSPA8/HSC70 is depicted separately.

(B and C) SH-SY5Y cell lines (B) stably expressing Flag-HA-USP14 and Flag-HA-GFP, (C) transiently expressing wild-type and mutant USP14 construct (WT-USP14 and W58A-USP14) were analyzed by immunoblotting for HSC70 and Flag expression. Actin served as loading control.

SH-SY5Y cells overexpressing various USP14 constructs were treated with drugs and analyzed for the interaction with HSC70.

(D) Flag-WT-USP14 and Flag-W58A-USP14 constructs.

(E) Flag-WT-USP14 and treatment with the proteasome inhibitor, bortezomib (0.5 μM, 6 h). Treatment with DMSO was used as a negative control.

(F) Flag-WT-USP14 or Flag-W58A-USP14 co-expressed with GFP-WT-HSC70 were treated with MG132 (20 μM, 6 h) or DMSO (negative control) and subjected to IP with anti-Flag antibodies.

The immunoprecipitated complexes were analyzed by IB for HSC70 and Flag (D and E) and for GFP, and Flag (F) values represent means ± SEM, n = 3. (B) p value was calculated by student's t-test and (C) one-way ANOVA. *$p \leq 0.05$; ****$p \leq 0.0001$.

FASP, filter-aided sample preparation; nanoLC-MS/MS, nano-liquid chromatography coupled tandem mass spectrometry; Co-IP, co-immunoprecipitation; SAINT, significance analysis of interactome; USP14, ubiquitin-specific protease-14; WT, wild-type; IB, immunoblotting; HSPA8/HSC70, heat shock cognate 71 kDa protein; HA, hemagglutinin tag; GFP, green fluorescent protein.

signaling cascades during UPR and ER stress including the splicing of the X-box binding protein 1 (XBP1) mRNA producing the transcription factor XBP1s (Lee et al., 2008). The unspliced mRNA is still translated into a functional protein (called XBP1u, unspliced XBP1) in higher order eukaryotes (Tirosh et al., 2006). To investigate whether USP14 interacts with the XBP1 proteins, we studied endogenous USP14 in primary cortical neurons (Do et al., 2013). As shown by immunoprecipitation, USP14 interacted with XBP1, but only with the 29 kDa, unspliced XBP1 form (XBP1u, marked with a red star in Figure 3A) under normal conditions, and this interaction was more pronounced upon MG132-induced proteasome inhibition (Figure 3A, lane 2). To further assess this interaction, co-immunoprecipitation experiments were performed in SH-SY5Y cells expressing Myc-DDK-XBP1u followed by immunoprecipitation using anti-Flag antibody. XBP1u preferentially interacted with USP14 under conditions of proteasome inhibition by MG132 (Figure 3B). This interaction was more pronounced by overexpression of WT-USP14 leading to the appearance of HSC70 in the formed immunocomplex (Figure 3B, lane 4). This suggests the existence of a tri-partite complex of XBP1u, USP14, and HSC70 present after proteasome inhibition in the cells. Next, we performed immunoprecipitation experiments in SH-SY5Y cells using Flag-tagged USP14 constructs showing that WT-USP14 and the UBL-mutant, W58A-USP14, did not significantly bind XBP1u under unstressed control conditions (Figure 3C, lane 1 and 4). However, upon proteasome inhibition that elevates XBP1u, there was a clear interaction of XBP1u with WT-USP14 (Figure 3C, lane 3). In these experiments, addition of tunicamycin did not induce the USP14-XBP1u interaction. These results reveal that USP14 interacts with XBP1u upon inhibition of the proteasome with potential functional consequences on ER stress regulation and crosstalk between different cellular processes.

XBP1u Forms Aggresome-like Induced Structures upon Proteasome Inhibition in Neuroblastoma Cells

Based on the findings above, we investigated the dynamics of XBP1u upon proteasome inhibition. Toward this goal, SH-SY5Y cells were treated with MG132 or the lysosomal inhibitor, chloroquine, followed by immunoblotting using anti-XBP1 antibody (representative immunoblot in Figure 4A depicts XBP1u detected by XBP1 antibody). MG132 induced a robust increase in protein levels of XBP1u, whereas chloroquine treatment had a minor effect on XBP1u (Figure 4A). To clarify whether USP14 influences the increase in XBP1u upon proteasome inhibition, we expressed GFP-WT-USP14 in neuroblastoma cells further treated with either MG132 or bortezomib (Figure 4B). USP14 overexpression did not affect the protein levels of XBP1u induced by these inhibitors (Figure 4B). Next, immunostainings using specific anti-XBP1u antibody were performed to assess the cellular localization of XBP1u in control and proteasome-inhibited SH-SY5Y cells (Figure 4C). We observed that XBP1u was present in aggresome-like induced structures (named here ALIS) in the MG132-treated neuroblastoma cells. We then generated stable SH-SY5Y cell lines with downregulation of USP14 using specific shRNA constructs, whereas control cells were created using scrambled shRNA. The level of USP14 protein in the USP14-shRNA cell lines was efficiently downregulated, by ~70%–80% in comparison to control cells. Most significantly, the increase in XBP1u induced by MG132 was significantly reduced in the USP14-deficient cells (Figure 4D). Together, these findings demonstrate that XBP1u accumulates in neuroblastoma cells after proteasome inhibition and that XBP1u levels are affected by the expression of USP14.

USP14 Levels Affect IRE1α Phosphorylation and Splicing of XBP1

It was previously reported that XBP1u nascent polypeptide can influence the localization of its own mRNA to the ER membrane, facilitating the generation of spliced XBP1 by IRE1α (Yanagitani et al., 2009). Given the role of USP14 in regulation of XBP1u levels, we investigated the function of USP14 in modulating IRE1α response following proteasome inhibition. Overexpression of Flag-WT-USP14 in SH-SY5Y cells followed by immunoprecipitation showed that USP14 interacts with IRE1α upon proteasome inhibition (Figure 5A). The interaction following tunicamycin treatment was also detected, but to a significantly lesser degree, whereas the effect of MG132 was more pronounced (Figure 5A). Treatment of USP14-shRNA knockdown cell lines with MG132 produced a large increase in the phosphorylation of IRE1α as shown by the ratio of phosphorylated to total IRE1α (Figure 5B). The level of spliced XBP1 (XBP1s) was also increased following MG132 treatment; however, this increase was reduced in the USP14-deficient neuroblastoma cells (Figure 5B). Next, we investigated the effects of tunicamycin in the USP14-shRNA knock-down cell lines. Addition of tunicamycin for 6 h induced IRE1α phosphorylation and XBP1s reflecting the activation of the UPR (Figure 5C). In contrast to MG312, the effect of tunicamycin on IRE1α phosphorylation was reduced in USP14-deficient cells (Figure 5C), whereas the level of XBP1s was the same in control and USP14 downregulated cells treated with tunicamycin. This shows that the downregulation of USP14 differentially affects

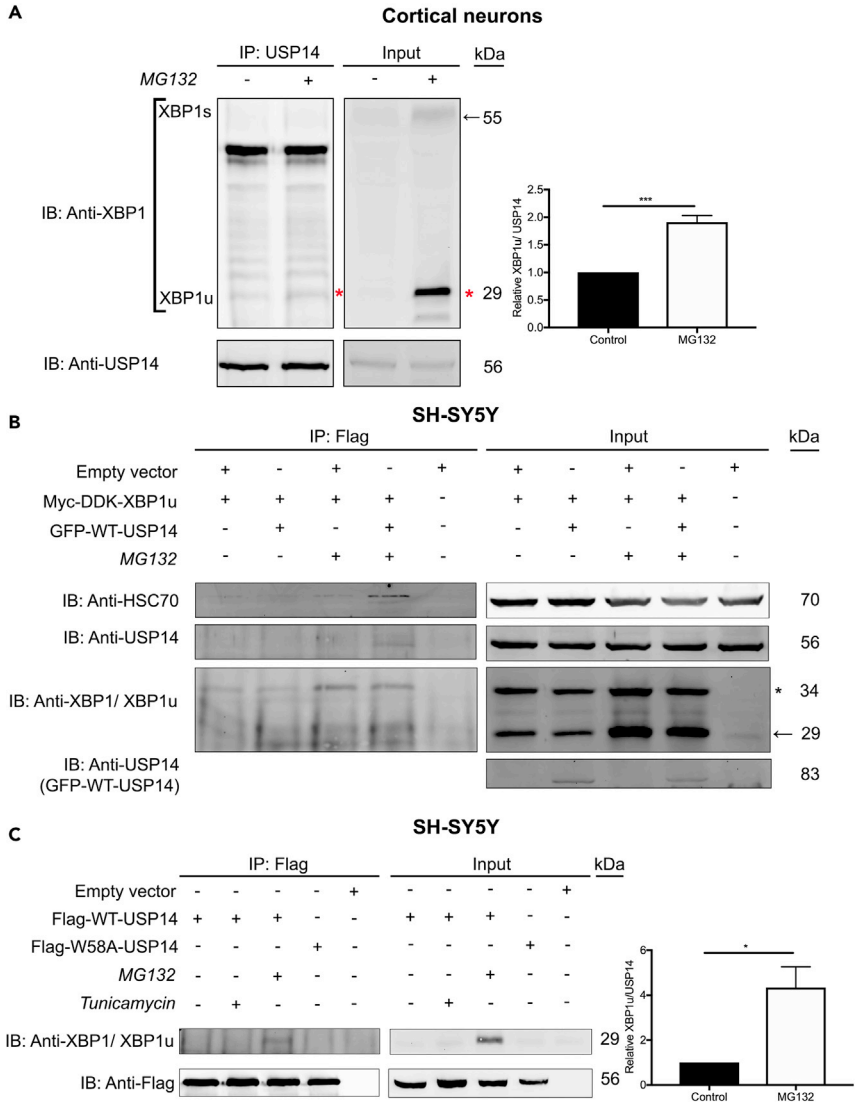

Figure 3. USP14 Associates with XBP1u upon Proteasome Inhibition

(A) Rat primary cortical neurons were treated for 6 h with MG132 (20 μM) or DMSO, lysed, and subjected to IP utilizing anti-USP14 antibody. Right panel depicts a histogram for the densitometry ratio XBP1u (red *)-USP14 interaction in the pull down.
(B) SH-SY5Y cells overexpressing Myc-DDK-XBP1u and treated for 6 h with MG132 (20 μM) in the presence and absence of GFP-WT-USP14 were subjected to IP with anti-Flag antibody. Treatment with DMSO served as a negative control.
(C) SH-SY5Y cells overexpressing Flag-WT-USP14 or Flag-W58A-USP14 were treated for 6 h with MG132 (20 μM) or tunicamycin (2.5 μg/mL) and immunoprecipitated with anti-Flag antibody. Treatment with DMSO served as negative control. Right panel depicts a histogram for the densitometry ratio of XBP1u normalized to Flag in the pull down.
The complexes were analyzed by immunoblotting for (A) USP14 and XBP1 (XBP1u) (B) USP14, HSC70, and XBP1 (XBP1u), (C) XBP1 (XBP1u), and Flag. XBP1u-unspliced X-box-binding protein 1. (A) n = 4, (C) n = 3. p value was calculated by student's t-test (A and C). *$p \leq 0.05$; ***$p \leq 0.001$.

IRE1α signaling in the cell upon proteasome inhibition, increasing the degree of IRE1α phosphorylation, whereas reducing the levels of XBP1s.

USP14 Is Reduced in Striatal Neurons Expressing Mutant Htt Cells

We previously observed that overexpression of USP14 decreased the amount of mutant Htt aggregates in neuronal cells, partly due to its beneficial effects on reducing ER stress (Hyrskyluoto et al., 2014). However, the role of endogenous USP14 in striatal neurons that are the main target in HD remained unclear. To resolve this, we cultured striatal cells expressing endogenous wild-type Htt (7Q repeats) or mutant

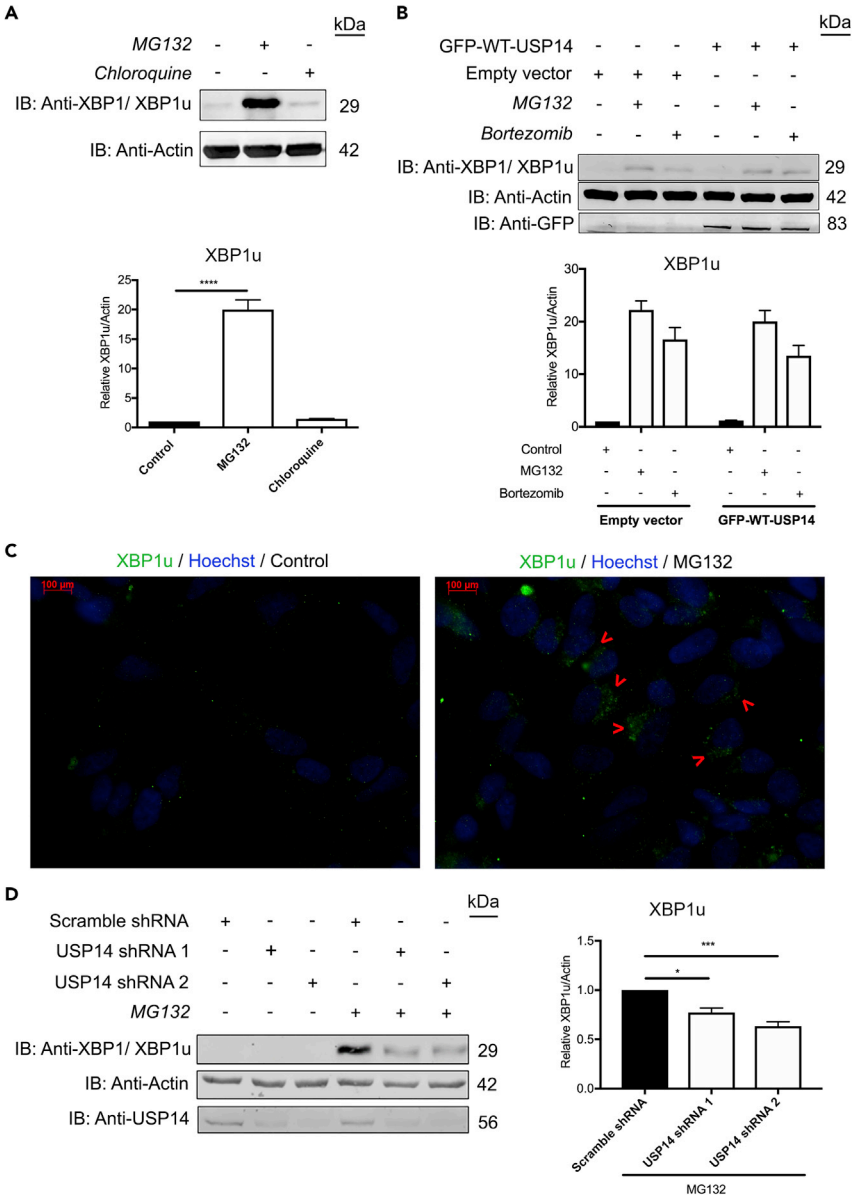

Figure 4. XBP1u Is Increased upon Proteasome Inhibition and Forms ALIS Structures in Cells Regulated by USP14

(A) SH-SY5Y cells treated with MG132 (20 μM), chloroquine (50 μM), or DMSO (negative control) for 6 h were analyzed by immunoblotting for the presence of XBP1u detected by XBP1 antibody. Lower panel depicts densitometry histograms for the value of XBP1u normalized to actin.

(B) SH-SY5Y cells transfected with GFP-WT-USP14 or empty vector were treated with MG132 (20 μM), bortezomib (0.5 μM), or DMSO for 6 h (negative control) and analyzed for the presence of XBP1u. Immunodetection with anti-GFP and anti-actin served as transfection and loading controls, respectively. Lower panel shows XBP1u normalized to actin.

(C) SH-SY5Y cells treated with MG132 (20 μM) or DMSO for 6 h were fixed and stained with anti-XBP1u antibodies. Note presence of immunopositive aggregates, named aggresome-like induced structures (ALIS, green). Nuclei were stained by Hoechst dye (blue). Scale bar, 100 μm.

(D) USP14 shRNA and scramble shRNA lentivirus-infected SH-SY5Y cells were treated with MG132 (20 μM) or DMSO for 6 h. The lysates were analyzed by IB for XBP1 (XBP1u), actin, and USP14. Right panel depicts a histogram for the densitometry ratio of XBP1u normalized to actin.

n = 3, p value was calculated by one-way (A and D) or two-way ANOVA (B). *$p \leq 0.05$; ***$p \leq 0.001$, ****$p \leq 0.0001$.

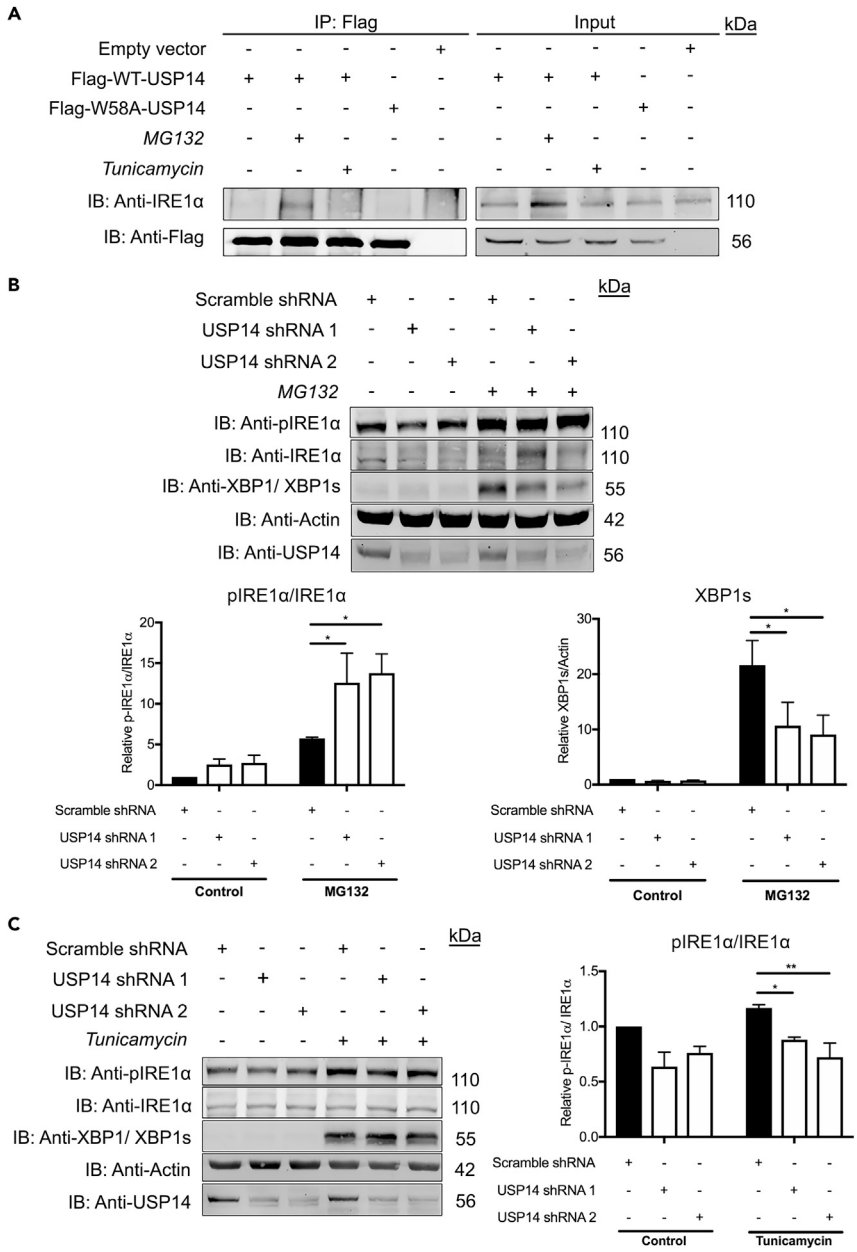

Figure 5. USP14 Differentially Regulates IRE1α upon Proteasomal Inhibition

(A) SH-SY5Y cells overexpressing Flag-WT-USP14 or Flag-W58A-USP14 and treated for 6 h with MG132 (20 μM) or tunicamycin (2.5 μg/mL) were subjected to IP with anti-Flag antibodies. Immunoprecipitated complexes were analyzed for the presence of IRE1α and Flag.

USP14 shRNA and scramble shRNA lentivirus-infected SH-SY5Y cells were treated with (B) MG132 (20 μM) or (C) tunicamycin (2.5 μg/mL) for 6 h. Treatment with DMSO served as negative control. The lysates were analyzed for the presence of IRE1α, p-IRE1α, and XBP1s (detected by XBP1 antibody). Immunodetection with anti-USP14 and anti-actin served as a control for silencing efficiency and loading control, respectively. (B) Lower panel depicts densitometry histograms for the ratio of p-IRE1α normalized to total IRE1α and XBP1s normalized to actin. (C) Densitometry ratio of p-IRE1α normalized to total IRE1α.

(B and C) n = 3, p value was calculated by two-way ANOVA. *$p \leq 0.05$; **$p \leq 0.01$. IRE1α, inositol-requiring protein 1α; XBP1s, spliced X-box-binding protein 1; pIRE1α, phosphorylated IRE1α.

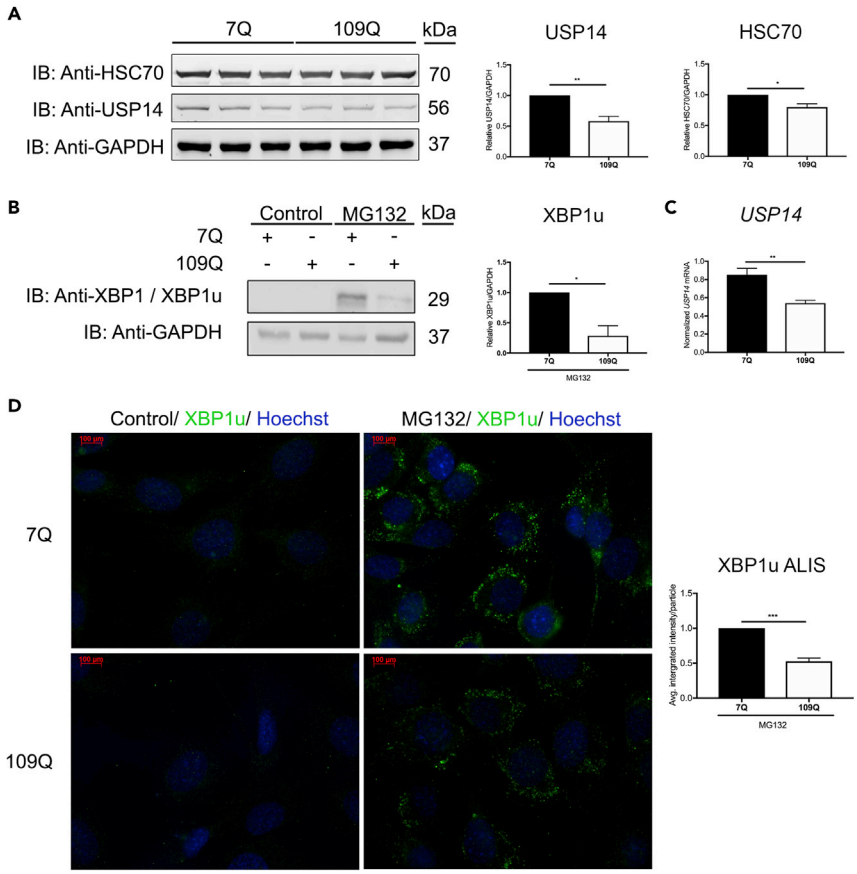

Figure 6. Striatal Cells Expressing Mutant Htt Have Reduced Levels of USP14, HSC70, and XBP1u Aggregates

(A) Striatal cells expressing 7Q (control) and 109Q (mutant) huntingtin (Htt) were subjected to immunoblotting for USP14, HSC70, and GAPDH. Lower panels represent histograms of the densitometry ratios of USP14 and HSC70, normalized to GAPDH.

(B) Striatal cells expressing 7Q or 109Q Htt were treated with MG132 (20 μM, 6 h) or DMSO (control) followed by immunoblotting for XBP1u using anti-XBP1 antibody. Right panel represents the histogram for the densitometry ratio of XBP1u normalized to GAPDH.

(C) qPCR was done as described in Transparent Methods. Note reduced expression of *USP14* in 109Q Htt cells compared with 7Q Htt cells. Gene expression was normalized to *GAPDH* and controls set to 1.

(D) Striatal cells were immunostained for XBP1u to show presence of XBP1u-positive ALIS induced by MG132. Note reduced immunostaining in 109Q Htt cells compared with 7Q Htt cells. Right panel represents a histogram for the average integrated intensity per XBP1u particle. Nuclei were stained by Hoechst dye (blue). Scale bar, 100 μm.

In (A–D, except C) n = 3, (C) n = 5, (A–D) p value was calculated by Student's t-test. *p ≤ 0.05, **p ≤ 0.01, ***p ≤ 0.001. 7Q, 7-polyglutamine repeats; 109Q, 109-polyglutamine repeats; GAPDH, glyceraldehyde 3-phosphate dehydrogenase.

Htt (109Q repeats) proteins (Kannike et al., 2014; Zuccato et al., 2003). Immunoblotting showed that USP14 levels together with HSC70 were reduced in striatal cells expressing mutant 109Q Htt compared with controls (Figure 6A). Quantitative PCR analyses done as in Pham et al. (2019) revealed that USP14 expression was also lowered in mutant Htt cells (Figure 6C). As in neuroblastoma cells (Figure 4), treatment with MG132 induced an increase in XBP1u in control striatal cells (Figure 6B). However, this increase was significantly less pronounced in mutant Htt-expressing cells (Figure 6B). Immunostaining of these cells revealed that the formation of XBP1u containing ALIS induced by MG132 was also reduced in mutant Htt cells (Figure 6D).

Inhibition of HSC70 Reduces the Cell Viability and Downregulates USP14 in Striatal Cells

Earlier reports on the role of HSC70 chaperone in neurodegenerative diseases revealed its function in disaggregating misfolded proteins and in autophagy processes (Scior et al., 2018; Tekirdag and Cuervo, 2018). To study the role of HSC70 in interaction with USP14, we employed VER-155008, a small molecule

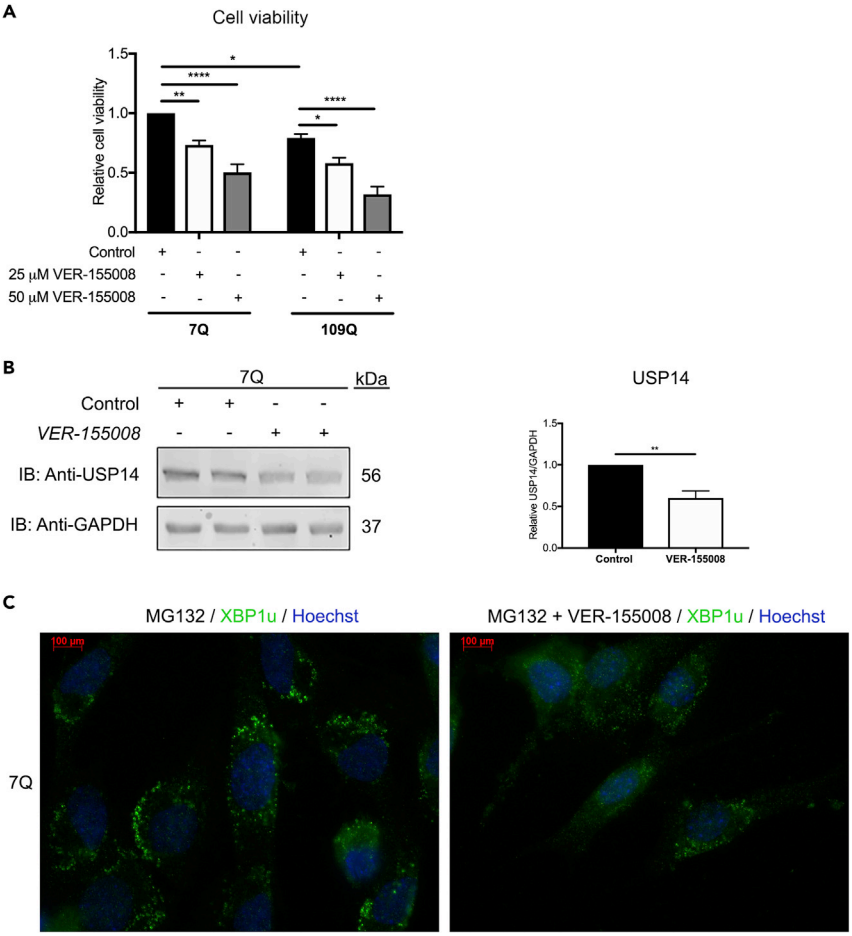

Figure 7. Chemical Inhibition of HSC70 with VER-155008 Causes Cell Death in Striatal Neuronal Cells and Downregulates USP14 Protein Levels

(A) Striatal cells expressing 7Q or 109Q Htt were treated with VER-155008 (25 μM or 50 μM, 24 h). Cell viability was assessed with MTT as described in Transparent Methods.

(B) Striatal 7Q Htt cells were stimulated with VER-155008 (25 μM, 24 h) and the lysates analyzed for the presence of USP14. Right panel shows histogram for the densitometry ratio of USP14 normalized to GAPDH.

(C) Striatal cells were immunostained for XBP1u to show the effect of VER-155008 on MG132-induced XBP1u ALIS in 7Q Htt-expressing cells. Nuclei were stained by Hoechst dye (blue). Scale bar, 100 μm.

p value calculated by two-way ANOVA n = 4 (A), Student's t-test n = 3 (B). *$p \leq 0.05$, **$p \leq 0.01$, ****$p \leq 0.0001$. MTT, 3-(4,5-dimethylthiazol-2-yl)-2,5-diphenyltetrazolium bromide.

Nuclei were stained by Hoechst dye (blue). Scale bar, 100 μm.

inhibitor of HSC70 (Yang and Tohda, 2018). VER-155008 induced a significant amount of cell degeneration in cultured striatal cells in a dose-dependent manner, and mutant cells expressing 109Q Htt were generally more vulnerable to the effect of VER-155008 (Figure 7A). Treatment with VER-155008 also reduced the level of USP14 in the striatal cells (Figure 7B). Further corroborating the role of HSC70 in USP14 dynamics, VER-155008 downregulated the XBP1u ALIS structures in striatal cells following proteasome inhibition (Figure 7C). Taken together, these results show that inhibition of HSC70 by VER-155008 reduced viability of striatal cells in conjunction with a decrease in USP14 and with an influence on MG132-induced XBP1u ALIS.

W58A-USP14 Interacts with GABARAP and Enhances the Formation of GABARAP Positive Autophagosomes that Are Regulated by VER-155008

Proteasome inhibition has been linked to an increase in compensatory autophagy establishing a functional crosstalk between the two cellular processes (Kim et al., 2018; Kocaturk and Gozuacik, 2018; Sha et al., 2018). Several proteins including the autophagy-related protein 8 (Atg8) family, involved in the formation

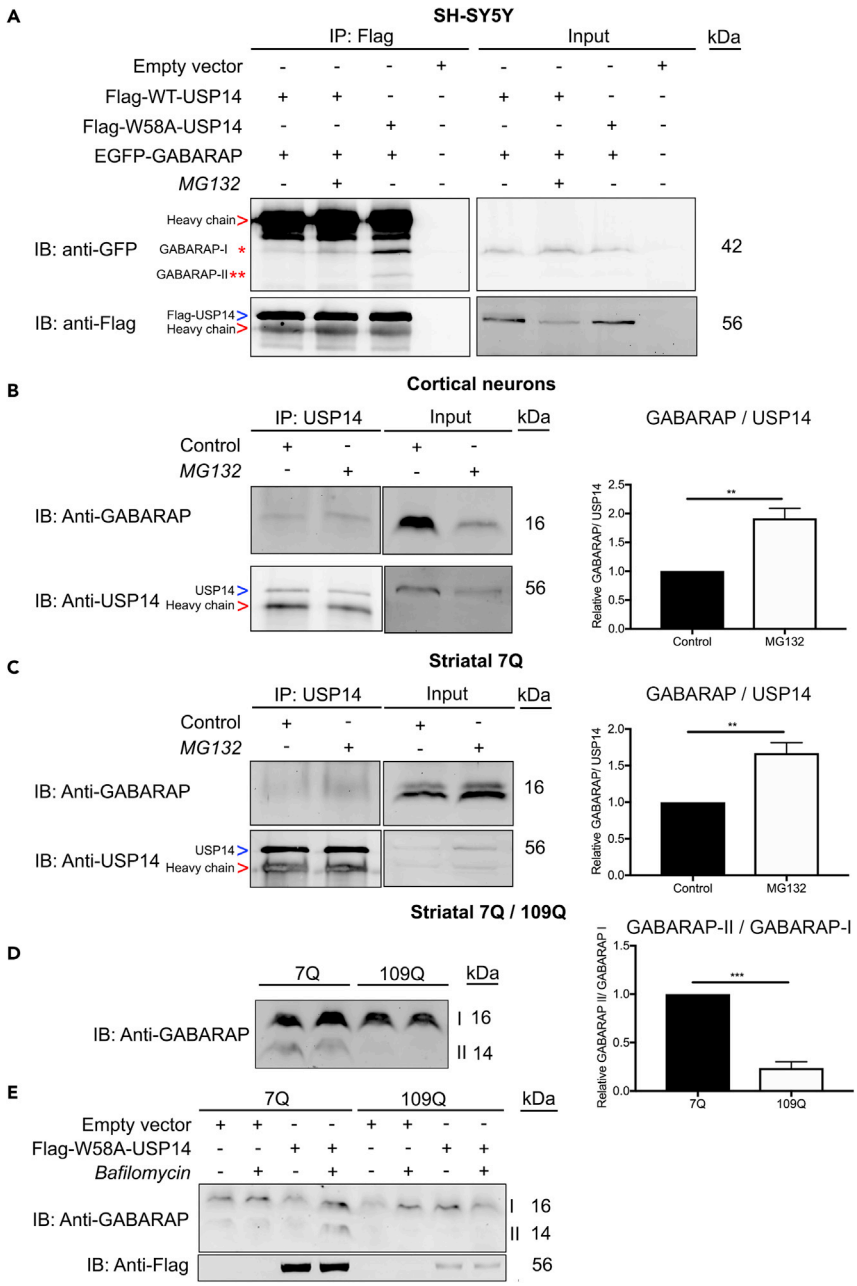

Figure 8. Proteasome Inhibition or Expression of Mutant W58A-USP14 Increases Association of USP14 with GABARAP in Neuronal Cells

(A) SH-SY5Y cells overexpressing Flag-WT-USP14 or Flag-W58A-USP14 together with EGFP-GABARAP were treated with MG132 (20 μM, 6 h) and subjected to IP with anti-Flag antibody. The complexes were analyzed by immunoblotting using anti-GFP and anti-Flag antibodies. Red arrow indicates IgG heavy chain band. Blue arrow indicates Flag-USP14. (Red *)—pro form of GABARAP (GABARAP-I), (Red **)—mature form of GABARAP (GABARAP-II).

(B) Primary cortical neurons were treated with MG132 (20 μM, 6 h) or DMSO and subjected to IP with anti-USP14 antibody. The complexes were analyzed with anti-GABARAP and anti-USP14 antibodies. Red arrow indicates IgG heavy chain band. Blue arrow indicates USP14.

(C) Striatal 7Q cells were treated with MG132 (20 μM, 6 h) or DMSO and subjected to IP with anti-USP14 antibody. The complexes were immunoblotted for anti-GABARAP and anti-USP14 antibodies. Red arrow indicates IgG heavy chain band. Blue arrow indicates USP14.

In (B and C) right panel represents histogram for the densitometry ratio of GABARAP to USP14 in the pull down.

Figure 8. *Continued*

(D) Striatal cells expressing 7Q (control) and 109Q (mutant) Htt were subjected to immunoblotting for GABARAP. Right panel represents histograms for the densitometry ratio of GABARAP-II/GABARAP-I.

(E) Striatal cells expressing 7Q and 109Q Htt and transfected with Flag-W58A-USP14 were stimulated with bafilomycin (200 nM, 6 h). Cell lysates were analyzed with IB for anti-GABARAP and anti-Flag.

In (B–D) n = 3, p value was calculated by Student's t-test. **p ≤ 0.01, ***p ≤ 0.001. GABARAP- GABA type A receptor-associated protein.

of the autophagosomal membrane at different stages, regulate autophagy. Mammalian Atg8 genes consist of three subfamilies: microtubule-associated protein 1 light chain 3 (LC3), γ-aminobutyric-acid-receptor-associated protein (GABARAP) and Golgi-associated ATPase enhancer of 16 kDa (GATE-16) (Shpilka et al., 2011). Using co-immunoprecipitation, we studied whether USP14 can interact with GABARAP, which is involved in the maturation of autophagosomes. Results showed that there was a weak interaction of GABARAP with WT-USP14 in the neuroblastoma cells under normal conditions (Figure 8A, lane 1). However, the strength of the interaction was more pronounced upon proteasome inhibition using MG132 (Figure 8A, lane 2), and the UBL-mutant, W58A-USP14, avidly interacted with GABARAP even without addition of MG132 (Figure 8A, lane 3). Validation of the protein interaction was achieved in primary cortical neurons (Figure 8B) and striatal neuronal cells (Figure 8C), corroborating that proteasome inhibition increased the association of endogenous USP14 with GABARAP compared with controls (lane 1, Figures 8B and 8C). To study the functional consequences of the USP14-GABARAP interaction, we focused on the striatal neuronal cells expressing either 7Q Htt or 109Q mutant Htt. Immunoblotting revealed that GABARAP was downregulated in the 109Q Htt cells (Figure 8D). GABARAP, as other ATG8 family proteins, is processed to a mature form GABARAP-II, aiding in autophagosome formation, and this was reduced in the mutant 109Q cells, as shown by the densitometric ratio of GABARAP-II (mature form) to GABARAP-I (pro form) (Figure 8D, lane 3 and 4; right panel histogram). Bafilomycin is known to block the fusion of autophagosomes and lysosomes. Striatal 7Q-cells expressing W58A-USP14 and treated with bafilomycin displayed an increased conversion of GABARAP during autophagy (Figure 8E, lane 4), indicating that W58A-USP14 could regulate this process. However, in the 109Q mutant Htt cells, there was no clear increase in GABARAP processing in the presence of neither W58A-USP14 nor bafilomycin (Figure 8E, lane 8). To investigate this further, we used live cell imaging of EGFP-GABARAP positive puncta as representative of autophagosomes present in the striatal cells after different treatments (Figures 9A–9C). Striatal 7Q-expressing cells exhibited more GABARAP-positive puncta compared with 109Q-expressing cells (Figures 9A–9C). Addition of chloroquine to block lysosomal degradation increased the number of these structures, particularly in control 7Q-expressing cells (Figure 9A). W58A-USP14 expression also increased the GABARAP-positive puncta, which was further elevated by the addition of chloroquine (Figure 9A, panels 3 and 4). Next, we studied whether HSC70 could play a role in the W58A-USP14 mediated increase in GABARAP-positive puncta. Addition of VER-155008 to inhibit HSC70 blocked the increase in GABARAP-positive puncta that arose from W58A-USP14 expression (Figure 9B, panels 2 and 3). To study the GABARAP positive autophagosomal structures at a higher resolution we then employed the Nikon Eclipse Ti-E inverted wide-field microscope equipped with an environmental chamber (see Transparent Methods). This set of imaging confirmed the increase in GABARAP-positive puncta by W58A-USP14 (Figure 9C, panel 2), as well as the decrease following the inhibition of HSC70 with VER-155008 (Figure 9C, panel 2 and 3). Together the live cell experiments demonstrate that HSC70 can influence GABARAP-positive puncta in the striatal cells and likely so via its interaction with USP14. The results further suggest that mutant Htt-expressing striatal cells have a defect in autophagy at the GABARAP-mediated autophagosome maturation level. As shown here this can be modulated by USP14 and HSC70 proteins, which can be of significance in HD and other neurodegenerative diseases accompanied by a dysfunctional autophagy.

DISCUSSION

In this work, we demonstrate that USP14 plays a role in regulation of autophagy and UPR in neuronal cells. The basis for this is the ability of USP14 to constitute functional protein-protein interactions with key signaling molecules in the cell. The precise nature of such modules involving USP14 has so far remained elusive except for reports on the binding of USP14 to Beclin-1 (Xu et al., 2016), c-Jun (Vaden et al., 2015), and IRE1α (Hyrskyluoto et al., 2014), and the molecular mechanisms associated with these interactions are not fully understood. Using advanced proteomics, we show here that USP14 interacts with the molecular chaperone HSC70 in human neuroblastoma SH-SY5Y cells, which was functionally validated using immunoprecipitation and other experiments. The interaction between USP14 and HSC70 was enhanced

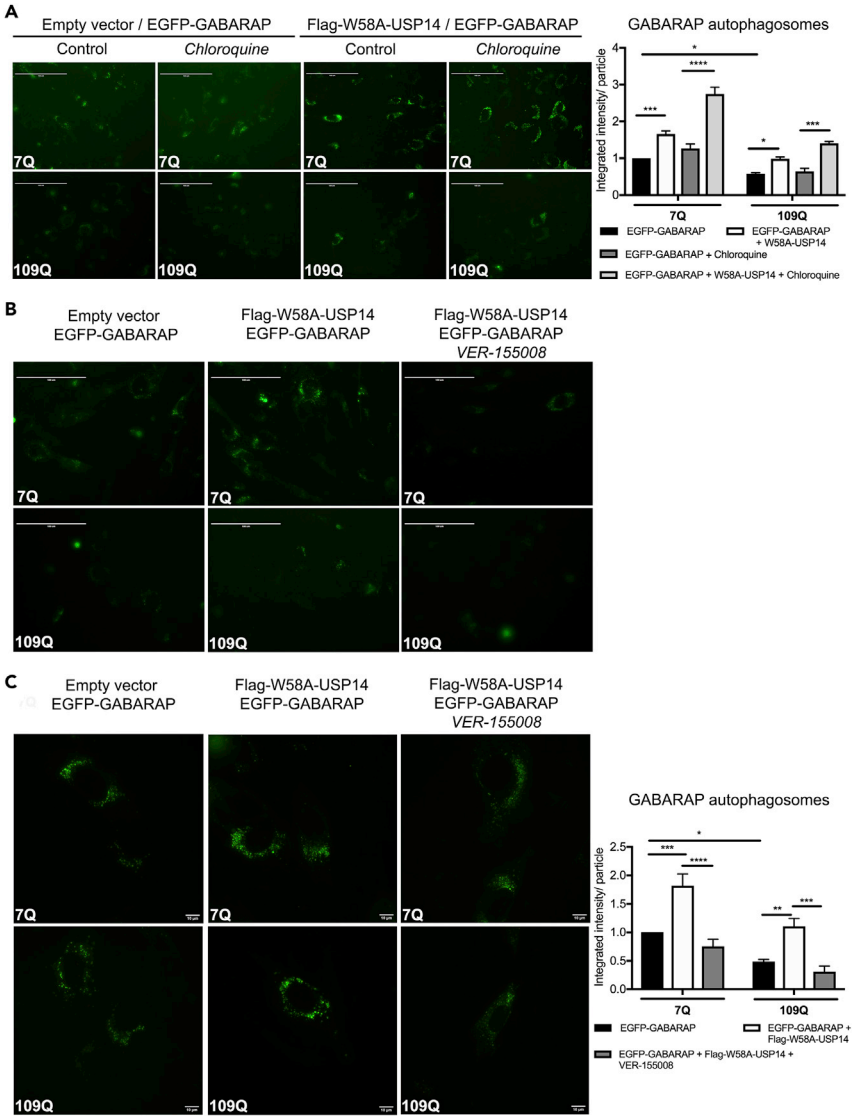

Figure 9. Mutant W58A-USP14 Increases GABARAP Positive Puncta in a HSC70-dependent Manner

(A and B) Striatal cells were transfected with EGFP-GABARAP in combination with an empty vector or Flag-W58A-USP14 and further stimulated with (A) chloroquine (50 μM, 5 h) or (B) VER-155008 (25 μM, 24 h). Live cell imaging was done using EVOS FL microscope revealing EGFP-GABARAP positive autophagosomes. In (A) right panel represents average integrated intensity per GABARAP particles depicted as a histogram. Intensity of GABARAP positive autophagosomal structures was quantified using ImageJ. n = 3. Scale, 100 μM (A and B).

(C) Striatal cells were plated on Ibidi ibitreat polymer bottom wells as described in Transparent Methods and transfected with EGFP-GABARAP in combination with an empty vector or Flag-W58A-USP14 and stimulated for 24 h with VER-155008 (25 μM). High-resolution live cell imaging with a Nikon-Eclipse Ti-E inverted wide-field microscope equipped with an environmental chamber was utilized to reveal the EGFP-GABARAP positive autophagosomes, n = 5. Scale, 10 μM.

In (A and C) p value was calculated by two-way ANOVA. *p ≤ 0.05, **p ≤ 0.01, ***p ≤ 0.001, ****p ≤ 0.0001.

EGFP,- enhanced green fluorescent protein.

by inhibition of the proteasome that reduced the binding of USP14 to the PSMD2 in the proteasome 19S RP. We further noticed that USP14 is able to interact with XBP1u and the ER-resident protein IRE1α. These findings demonstrate that with reduced binding to PSMD2, USP14 can interact with cellular proteins, such as HSC70, XBP1u, and IRE1α. These protein-protein interactions may have functional consequences in various human diseases characterized by accumulation of misfolded proteins and an impaired proteasome function. Particularly in HD and other polyQ diseases, expression of mutant proteins with expanded

repeats can block the proteasome and induce ER stress further exacerbating the disease conditions (Hyrskyluoto et al., 2013, 2014). Recent work also established that the expanded polyQ repeats inhibit Beclin-1 mediated autophagy (Ashkenazi et al., 2017). In this work, we have addressed the functionality of USP14 interactions specifically in the context of striatal neuronal cells expressing mutant Htt protein with dysregulated proteostasis and autophagy. USP14 is a vital component of the proteasome coordinating the deubiquitylation of protein substrates followed by substrate engagement, leading to proteasome activation (Peth et al., 2009). The mammalian 26S proteasome consists of two components, 19S RP and 20S core particle containing several subunits. USP14 binds to the PSMD2/RPN1 protein in the 19S RP via its N-terminal UBL domain (Aufderheide et al., 2015). Using mutagenesis, we have identified tryptophan at position 58 in the UBL domain of USP14 that disrupts the association of USP14 with PSMD2. The UBL-mutant W58A-USP14 behaved similarly to WT-USP14 upon proteasome inhibition indicating that they are functionally related. Results obtained with the W58A-USP14 mutant reinforce the concept of the existence of a dynamic pool of USP14 in the cell, performing proteasome independent functions in the cell.

To investigate the functions of USP14 independent of the proteasome, we first characterized its role in unfolded protein response based on its known interaction with the signaling protein IRE1α (Nagai et al., 2009). We have previously reported that USP14 counteracts the IRE1α-mediated ER stress and increases the clearance of mutant Htt in cells (Hyrskyluoto et al., 2014). In this study, we observed that the association of USP14 with IRE1α was further increased upon proteasome inhibition. Using USP14 knockdown cells we noted that USP14 deficiency resulted in an enhanced phosphorylation of IRE1α and a decrease in XBP1 splicing activity. This suggests that USP14 may differentially control the kinase and the RNase domain in IRE1α located at either ends of the molecule. Similar actions on IRE1α involving distinct responses in its structural domains have been reported for small molecule compounds that are ATP-competitive inhibitors that disrupt the IRE1α kinase function while activating the RNase domain (Feldman et al., 2016). It would be important to investigate whether the USP14 can serve as a determinant of IRE1α response upon different stimuli.

Subsequently, we noted that USP14 interacts with unspliced XBP1 (XBP1u) protein upon proteasome inhibition. Compared with spliced XBP1 acting as a transcription factor, less is known about XBP1u in cell physiology. Previous reports have shown that XBP1u is a short-lived protein (Tirosh et al., 2006), and XBP1u, via translational pausing of its nascent polypeptide, mediates efficient splicing of XBP1 mRNA by activated IRE1α upon ER stress (Kanda et al., 2016; Yanagitani et al., 2009). We observed that inhibition of the proteasome strongly upregulated XBP1u in neuronal cells with accumulation of the protein in aggresome-like induced structures, called here ALIS. These have been observed before in HEK 293T cells with no direct functions reported (Navon et al., 2010). We noted also that XBP1u interacts with USP14 and HSC70, likely forming a tri-partite complex in neuronal cells.

To investigate whether the ALIS are modulated in HD, we studied striatal cells expressing control 7Q or 109Q mutant Htt protein. To our surprise, we noticed that the mutant Htt expressing cells showed less formation of XBP1u positive ALIS upon proteasome inhibition compared with controls. These could be related to lowered levels of USP14 and HSC70 in the mutant cells. Treatment with the HSC70 inhibitor, VER-155008, reduced the formation of the ALIS in control striatal cells upon proteasome inhibition. Together, these findings indicate that ALIS formation is reduced in mutant Htt expressing cells and that USP14 along with HSC70 could be involved in their dynamics. Further studies are warranted to pinpoint the functions of the XBP1u positive ALIS in cell responses and in various diseases, such as HD.

HSC70 is a molecular chaperone that affects diverse cellular pathways by regulating protein folding and degradation of misfolded proteins. These processes are prone to dysfunction in human disorders with accumulation of misfolded or mutant proteins. In proteostasis, HSC70 is involved in the disaggregation of misfolded protein, in chaperone-mediated autophagy and in microautophagy (Tekirdag and Cuervo, 2018). USP14 binds Beclin-1 and inhibits the formation of autophagosomes by removing the K63-linked poly-ubiquitin chains on Beclin-1 (Xu et al., 2016). We hypothesized that USP14 along with HSC70 may play a role in modulating autophagy. For this purpose, we focused on GABARAP and its functions in autophagic processes. There are three ATG8 gene subfamilies in mammals, namely, microtubule-associated protein 1 light chain 3 (LC3), γ-aminobutyric-acid-receptor-associated protein (GABARAP), and Golgi-associated ATPase enhancer of 16 kDa (GATE-16) (Shpilka et al., 2011). GABARAP/GATE-16 is required for the formation of autophagosomes and their maturation (Weidberg et al., 2010a, 2010b), and further they can regulate $GABA_A$ receptor endocytosis, thus influencing

neuronal signaling function (Hui et al., 2019). The GABAergic medium spiny neurons in the striatum are particularly affected in HD. Hence, we investigated whether GABARAP along with USP14 and HSC70 could specifically have relevance in striatal neuronal cells expressing Htt.

To begin with, we noted that USP14 in the striatal cells expressing mutant Htt was decreased both at the mRNA and protein levels. The former may be related to reduced transcription, as accumulation of mutant Htt in the nucleus is known to affect gene expression; however, this warrants further investigation. We further observed that the protein levels of HSC70 were downregulated in the mutant Htt-expressing cells, and these cells were also more vulnerable to the action of VER-155008 inhibiting the activity of HSC70. These findings may indicate a possible role of HSC70 and its interaction with USP14 in the pathophysiology of HD. We further observed that the UBL-mutants, W58A-USP14 and WT-USP14, upon proteasome inhibition could interact with GABARAP in neuronal cells. Striatal neuronal cells expressing mutant Htt exhibited reduced conversion of GABARAP-I to its mature form, GABARAP-II. This indicated a possible defect in the GABARAP-mediated autophagosome maturation. To further characterize the physiological relevance of this we performed live cell imaging and tracking of EGFP-GABARAP positive autophagosomes in 7Q Htt and 109Q Htt expressing cells. Data showed that the formation of EGFP-GABARAP positive autophagosomes was downregulated in mutant Htt cells compared with control. Inhibition of lysosomes with chloroquine revealed that the mutant Htt-expressing cells exhibited a defect in GABARAP autophagosome biogenesis resulting in the reduced formation of these structures.

Overexpression of the UBL mutant, W58A-USP14, enhanced the formation of GABARAP positive autophagosomes in the striatal cells but also affected their clearance as demonstrated by using chloroquine. Most importantly, treatment with VER-155008 abrogated the USP14-mediated increase in GABARAP positive autophagosomal structures, signifying involvement of HSC70 in this process. Our findings indicate that HSC70 may have additional functions in the autophagy process beyond its established role in regulation of chaperone-mediated autophagy and microautophagy. Further studies are warranted to understand the dynamics of GABARAP and the importance of HSC70 and USP14 in autophagosome maturation.

In conclusion, we have identified proteasome-independent functions of USP14 in neuronal cells. USP14 interacts with the chaperone HSC70 and the protein XBP1u with functional consequences for coordination of ER signaling, upon proteasome inhibition and formation of GABARAP positive autophagosomes. We propose that the interaction of USP14 with HSC70 studied here can be considered a molecular hub for mediating cross-talk between the proteasome, ER stress signals, and autophagy in the cell (cartoon in graphical abstract). This hub could be a target for future drug development in different diseases including HD. Impairment of protein degradation involving the proteasomes as well as autophagy are key features of several human diseases including HD. Our results, using mutant Htt-expressing striatal neuronal cells, indicate that these cells have a defect in autophagy at the GABARAP sensitive stage of autophagosome maturation that can be influenced by USP14 and HSC70 proteins. Modulation of the USP14-HSC70 axis using different compounds could be a target for future drug development in neurodegenerative diseases including HD.

Limitations of the Study

Protein homeostasis (proteostasis) is crucial for proper cell function and viability and is known to be dysfunctional in several human diseases including cancer and neurodegenerative disorders. In our study, we have employed proteomic analyses and cell cultures to depict a role of the deubiquitinating enzyme USP14 in the control of proteostasis pathways via interaction with the chaperone, HSC70. Thereby we used a cell model to investigate the dysregulation of proteostasis and autophagy in Huntington disease. Further functional studies and *in vivo* models of HD and other disorders are required to confirm the precise role of the USP14-HSC70 axis in neuronal autophagy and in ER signaling as a possible target for modifying disease pathology.

METHODS

All methods can be found in the accompanying Transparent Methods supplemental file.

SUPPLEMENTAL INFORMATION

Supplemental Information can be found online at https://doi.org/10.1016/j.isci.2019.100790.

ACKNOWLEDGMENTS

Supported by Academy of Finland, Magnus Ehrnrooth Foundation, Liv och Hälsa Foundation Finska Läkaresällskapet, Parkinson- Säätiö, Finland, and Minerva Foundation for Medical Research, Finland. Proteomic analyses were performed at the Meilahti Clinical Proteomics Core Facility, HiLIFE supported by Biocenter Finland. Higher-resolution live cell imaging using Nikon Eclipse Ti-E wide-field inverted microscope was done at Biomedicum imaging unit (BIU), University of Helsinki. Packaging and generation of USP14 shRNA-expressing lentiviruses were performed at Biomedicum Functional Genomics Unit (FuGU), University of Helsinki.

We thank Kristina Söderholm for skillful technical assistance, Dr Tönis Timmusk and Dr Elena Cattaneo for striatal cells, Dr Pirta Hotulainen for primary neurons, Dr. Nikolai Engedal and Dr Anja Dröge for vector constructions, Dr Janusz Dębski and Prof. Michał Dadlez for mass spectrometric data analysis, and Prof. Anne-Claude Gingras for help with SAINT analysis. DL is a member of the EU Cost Action CA15138, Transautophagy.

AUTHOR CONTRIBUTIONS

V.S., C.B., M.L., and D.L. conceived and designed the experiments. V.S., C.B., and D.D.P. performed the experiments. V.S., E.S., R.S., M.L., and D.L. analyzed the data. V.S., M.L., and D.L. wrote the paper.

DECLARATION OF INTERESTS

The authors declare no competing interests to disclose.

Received: August 14, 2019
Revised: November 22, 2019
Accepted: December 13, 2019
Published: January 24, 2020

REFERENCES

Ashkenazi, A., Bento, C.F., Ricketts, T., Vicinanza, M., Siddiqi, F., Pavel, M., Squitieri, F., Hardenberg, M.C., Imarisio, S., Menzies, F.M., et al. (2017). Polyglutamine tracts regulate beclin 1-dependent autophagy. Nature *545*, 108–111.

Aufderheide, A., Beck, F., Stengel, F., Hartwig, M., Schweitzer, A., Pfeifer, G., Goldberg, A.L., Sakata, E., Baumeister, W., and Forster, F. (2015). Structural characterization of the interaction of Ubp6 with the 26S proteasome. Proc. Natl. Acad. Sci. U S A. *112*, 8626–8631.

Borodovsky, A., Ovaa, H., Kolli, N., Gan-Erdene, T., Wilkinson, K.D., Ploegh, H.L., and Kessler, B.M. (2002). Chemistry-based functional proteomics reveals novel members of the deubiquitinating enzyme family. Chem. Biol. *9*, 1149–1159.

Burckstummer, T., Bennett, K.L., Preradovic, A., Schutze, G., Hantschel, O., Superti-Furga, G., and Bauch, A. (2006). An efficient tandem affinity purification procedure for interaction proteomics in mammalian cells. Nat. Methods *3*, 1013–1019.

Cai, J., Xia, X., Liao, Y., Liu, N., Guo, Z., Chen, J., Yang, L., Long, H., Yang, Q., Zhang, X., et al. (2017). A novel deubiquitinase inhibitor b-AP15 triggers apoptosis in both androgen receptor-dependent and -independent prostate cancers. Oncotarget *8*, 63232–63246.

Chen, P.C., Qin, L.N., Li, X.M., Walters, B.J., Wilson, J.A., Mei, L., and Wilson, S.M. (2009). The proteasome-associated deubiquitinating enzyme Usp14 is essential for the maintenance of synaptic ubiquitin levels and the development of neuromuscular junctions. J. Neurosci. *29*, 10909–10919.

Ding, Y., Chen, X., Wang, B., Yu, B., and Ge, J. (2018). Deubiquitinase inhibitor b-AP15 activates endoplasmic reticulum (ER) stress and inhibits Wnt/Notch1 signaling pathway leading to the reduction of cell survival in hepatocellular carcinoma cells. Eur. J. Pharmacol. *825*, 10–18.

Do, H.T., Bruelle, C., Tselykh, T., Jalonen, P., Korhonen, L., and Lindholm, D. (2013). Reciprocal regulation of very low density lipoprotein receptors (VLDLRs) in neurons by brain-derived neurotrophic factor (BDNF) and Reelin: involvement of the E3 ligase Mylip/Idol. J. Biol. Chem. *288*, 29613–29620.

Feldman, H.C., Tong, M., Wang, L., Meza-Acevedo, R., Gobillot, T.A., Lebedev, I., Gliedt, M.J., Hari, S.B., Mitra, A.K., Backes, B.J., et al. (2016). Structural and functional analysis of the allosteric inhibition of IRE1alpha with ATP-competitive ligands. ACS Chem. Biol. *11*, 2195–2205.

Hui, K.K., Takashima, N., Watanabe, A., Chater, T.E., Matsukawa, H., Nekooki-Machida, Y., Nilsson, P., Endo, R., Goda, Y., Saido, T.C., et al. (2019). GABARAPs dysfunction by autophagy deficiency in adolescent brain impairs GABAA receptor trafficking and social behavior. Sci. Adv. *5*, eaau8237.

Hyrskyluoto, A., Pulli, I., Tornqvist, K., Ho, T.H., Korhonen, L., and Lindholm, D. (2013). Sigma-1 receptor agonist PRE084 is protective against mutant huntingtin-induced cell degeneration: involvement of calpastatin and the NF-kappaB pathway. Cell Death Dis *4*, e646.

Hyrskyluoto, A., Bruelle, C., Lundh, S.H., Do, H.T., Kivinen, J., Rappou, E., Reijonen, S., Waltimo, T., Petersen, A., Lindholm, D., et al. (2014). Ubiquitin-specific protease-14 reduces cellular aggregates and protects against mutant huntingtin-induced cell degeneration: involvement of the proteasome and ER stress-activated kinase IRE1alpha. Hum. Mol. Genet. *23*, 5928–5939.

Kanda, S., Yanagitani, K., Yokota, Y., Esaki, Y., and Kohno, K. (2016). Autonomous translational pausing is required for XBP1u mRNA recruitment to the ER via the SRP pathway. Proc. Natl. Acad. Sci. U S A. *113*, E5886–E5895.

Kannike, K., Sepp, M., Zuccato, C., Cattaneo, E., and Timmusk, T. (2014). Forkhead transcription factor FOXO3a levels are increased in Huntington disease because of overactivated positive autofeedback loop. J. Biol. Chem. *289*, 32845–32857.

Kim, E., Park, S., Lee, J.H., Mun, J.Y., Choi, W.H., Yun, Y., Lee, J., Kim, J.H., Kang, M.J., and Lee, M.J. (2018). Dual function of USP14 deubiquitinase in cellular proteasomal activity and autophagic flux. Cell Rep *24*, 732–743.

Kim, H.T., and Goldberg, A.L. (2017). The deubiquitinating enzyme Usp14 allosterically inhibits multiple proteasomal activities and ubiquitin-independent proteolysis. J. Biol. Chem. *292*, 9830–9839.

Kocaturk, N.M., and Gozuacik, D. (2018). Crosstalk between mammalian autophagy and the ubiquitin-proteasome system. Front. Cell Dev. Biol. *6*, 128.

Lappe-Siefke, C., Loebrich, S., Hevers, W., Waidmann, O.B., Schweizer, M., Fehr, S., Fritschy, J.M., Dikic, I., Eilers, J., Wilson, S.M., et al. (2009). The ataxia (axJ) mutation causes abnormal GABAA receptor turnover in mice. PLoS Genet. *5*, e1000631.

Lee, K.P., Dey, M., Neculai, D., Cao, C., Dever, T.E., and Sicheri, F. (2008). Structure of the dual enzyme Ire1 reveals the basis for catalysis and regulation in nonconventional RNA splicing. Cell *132*, 89–100.

Nagai, A., Kadowaki, H., Maruyama, T., Takeda, K., Nishitoh, H., and Ichijo, H. (2009). USP14 inhibits ER-associated degradation via interaction with IRE1alpha. Biochem. Biophys. Res. Commun. *379*, 995–1000.

Navon, A., Gatushkin, A., Zelcbuch, L., Shteingart, S., Farago, M., Hadar, R., and Tirosh, B. (2010). Direct proteasome binding and subsequent degradation of unspliced XBP-1 prevent its intracellular aggregation. FEBS Lett. *584*, 67–73.

Peth, A., Besche, H.C., and Goldberg, A.L. (2009). Ubiquitinated proteins activate the proteasome by binding to Usp14/Ubp6, which causes 20S gate opening. Mol. Cell *36*, 794–804.

Pham, D.D., Bruelle, C., Thi Do, H., Pajanoja, C., Jin, C., Srinivasan, V., Olkkonen, V.M., Eriksson, O., Jauhiainen, M., Lalowski, M., et al. (2019). Caspase-2 and p75 neurotrophin receptor (p75NTR) are involved in the regulation of SREBP and lipid genes in hepatocyte cells. Cell Death Dis *10*, 537.

Scifo, E., Szwajda, A., Debski, J., Uusi-Rauva, K., Kesti, T., Dadlez, M., Gingras, A.C., Tyynela, J., Baumann, M.H., Jalanko, A., et al. (2013). Drafting the CLN3 protein interactome in SH-SY5Y human neuroblastoma cells: a label-free quantitative proteomics approach. J. Proteome Res. *12*, 2101–2115.

Scifo, E., Szwajda, A., Soliymani, R., Pezzini, F., Bianchi, M., Dapkunas, A., Debski, J., Uusi-Rauva, K., Dadlez, M., Gingras, A.C., et al. (2015). Proteomic analysis of the palmitoyl protein thioesterase 1 interactome in SH-SY5Y human neuroblastoma cells. J. Proteomics *123*, 42–53.

Scior, A., Buntru, A., Arnsburg, K., Ast, A., Iburg, M., Juenemann, K., Pigazzini, M.L., Mlody, B., Puchkov, D., Priller, J., et al. (2018). Complete suppression of Htt fibrilization and disaggregation of Htt fibrils by a trimeric chaperone complex. EMBO J. *37*, 282–299.

Sha, Z., Schnell, H.M., Ruoff, K., and Goldberg, A. (2018). Rapid induction of p62 and GABARAPL1 upon proteasome inhibition promotes survival before autophagy activation. J. Cell Biol. *217*, 1757–1776.

Shpilka, T., Weidberg, H., Pietrokovski, S., and Elazar, Z. (2011). Atg8: an autophagy-related ubiquitin-like protein family. Genome Biol. *12*, 226.

Tekirdag, K., and Cuervo, A.M. (2018). Chaperone-mediated autophagy and endosomal microautophagy: Joint by a chaperone. J. Biol. Chem. *293*, 5414–5424.

Tirosh, B., Iwakoshi, N.N., Glimcher, L.H., and Ploegh, H.L. (2006). Rapid turnover of unspliced Xbp-1 as a factor that modulates the unfolded protein response. J. Biol. Chem. *281*, 5852–5860.

Vaden, J.H., Bhattacharyya, B.J., Chen, P.C., Watson, J.A., Marshall, A.G., Phillips, S.E., Wilson, J.A., King, G.D., Miller, R.J., and Wilson, S.M. (2015). Ubiquitin-specific protease 14 regulates c-Jun N-terminal kinase signaling at the neuromuscular junction. Mol. Neurodegener *10*, 3.

Weidberg, H., Shpilka, T., Shvets, E., and Elazar, Z. (2010a). Mammalian Atg8s: one is simply not enough. Autophagy *6*, 808–809.

Weidberg, H., Shvets, E., Shpilka, T., Shimron, F., Shinder, V., and Elazar, Z. (2010b). LC3 and GATE-16/GABARAP subfamilies are both essential yet act differently in autophagosome biogenesis. EMBO J. *29*, 1792–1802.

Xu, D., Shan, B., Sun, H., Xiao, J., Zhu, K., Xie, X., Li, X., Liang, W., Lu, X., Qian, L., et al. (2016). USP14 regulates autophagy by suppressing K63 ubiquitination of Beclin 1. Genes Dev. *30*, 1718–1730.

Yanagitani, K., Imagawa, Y., Iwawaki, T., Hosoda, A., Saito, M., Kimata, Y., and Kohno, K. (2009). Cotranslational targeting of XBP1 protein to the membrane promotes cytoplasmic splicing of its own mRNA. Mol. Cell *34*, 191–200.

Yang, X., and Tohda, C. (2018). Heat shock cognate 70 inhibitor, VER-155008, reduces memory deficits and axonal degeneration in a mouse model of Alzheimer's disease. Front. Pharmacol. *9*, 48.

Zuccato, C., Tartari, M., Crotti, A., Goffredo, D., Valenza, M., Conti, L., Cataudella, T., Leavitt, B.R., Hayden, M.R., Timmusk, T., et al. (2003). Huntingtin interacts with REST/NRSF to modulate the transcription of NRSE-controlled neuronal genes. Nat. Genet. *35*, 76–83.

iScience, Volume *23*

Supplemental Information

Dynamic Interaction of USP14 with the Chaperone HSC70 Mediates Crosstalk between the Proteasome, ER Signaling, and Autophagy

Vignesh Srinivasan, Celine Bruelle, Enzo Scifo, Dan Duc Pham, Rabah Soliymani, Maciej Lalowski, and Dan Lindholm

Supplemental Items

Figure S1

A

p-ES-NTAP-Puro vector

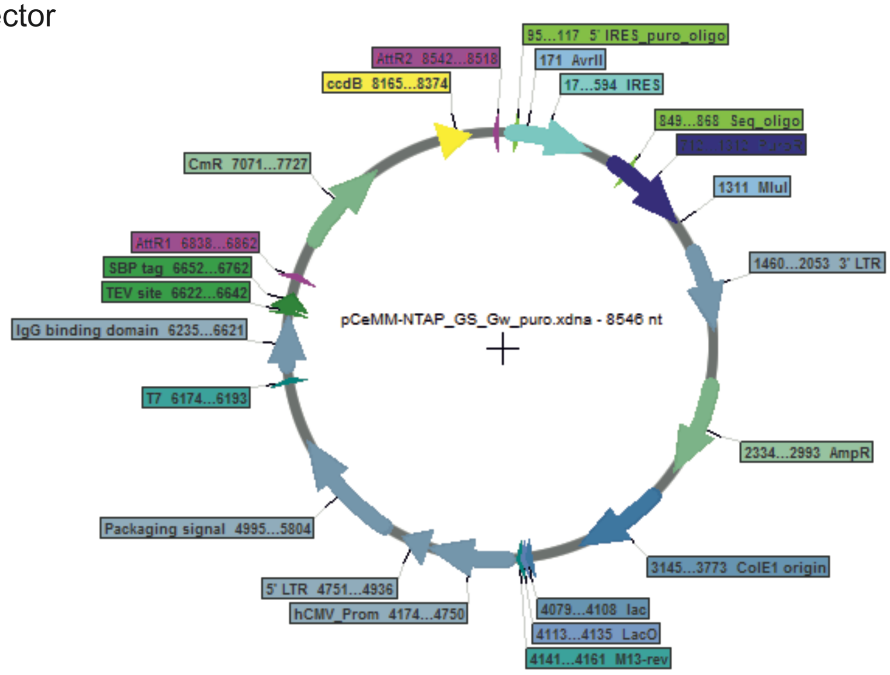

B

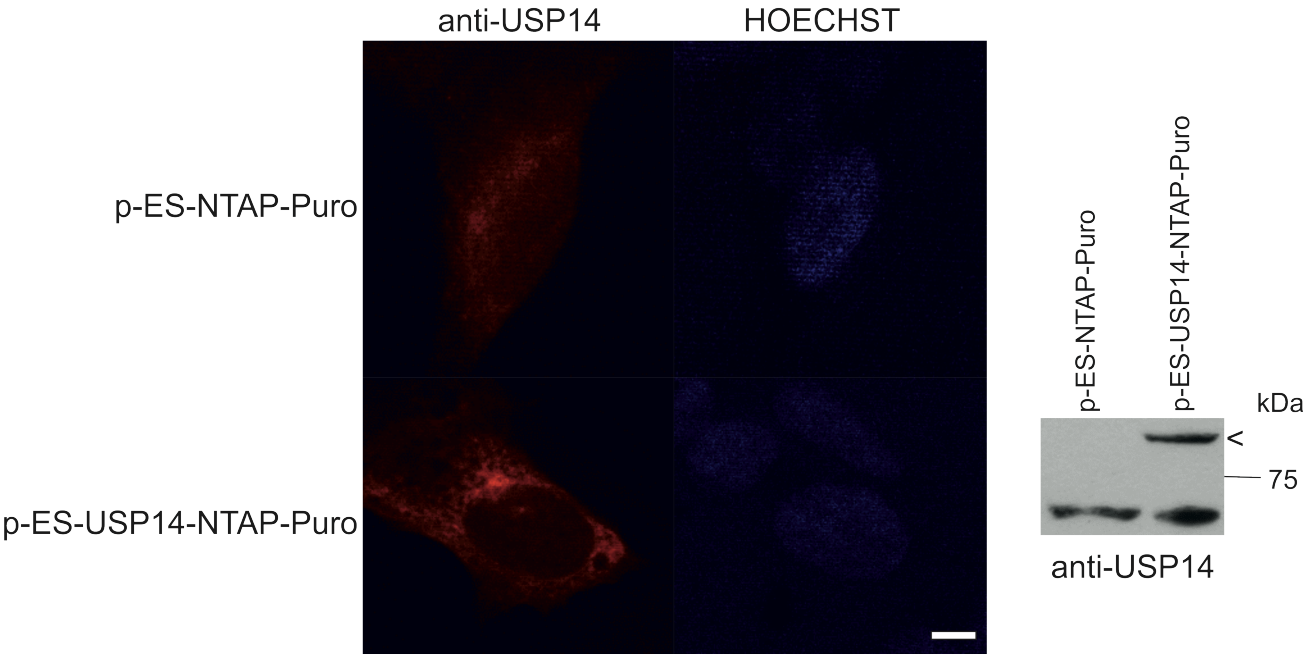

Figure S2

A

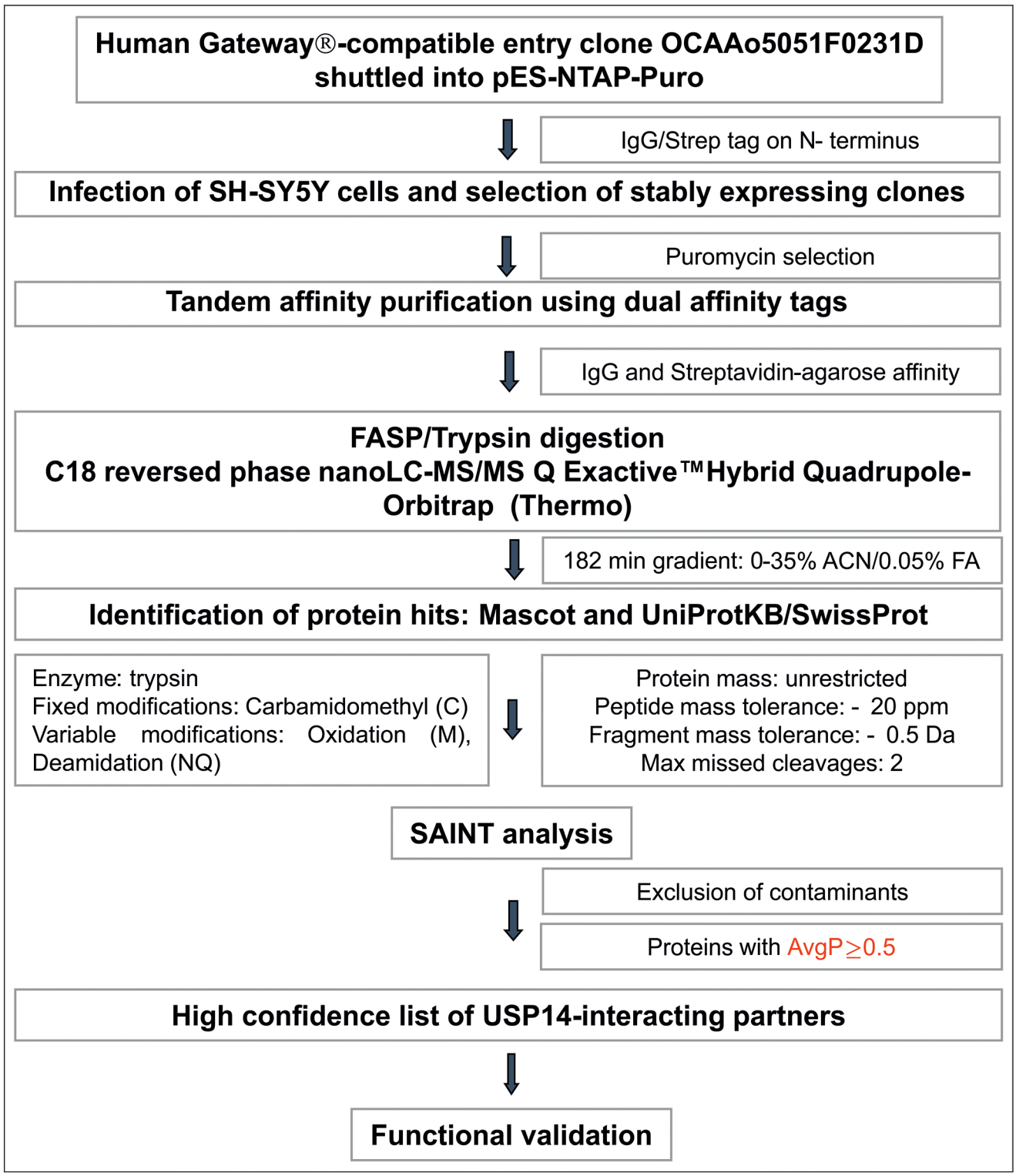
Human Gateway®-compatible entry clone OCAAo5051F0231D shuttled into pES-NTAP-Puro
IgG/Strep tag on N- terminus
Infection of SH-SY5Y cells and selection of stably expressing clones
Puromycin selection
Tandem affinity purification using dual affinity tags
IgG and Streptavidin-agarose affinity
FASP/Trypsin digestion
C18 reversed phase nanoLC-MS/MS Q Exactive™Hybrid Quadrupole-Orbitrap (Thermo)
182 min gradient: 0-35% ACN/0.05% FA
Identification of protein hits: Mascot and UniProtKB/SwissProt
Enzyme: trypsin
Fixed modifications: Carbamidomethyl (C)
Variable modifications: Oxidation (M), Deamidation (NQ)
Protein mass: unrestricted
Peptide mass tolerance: - 20 ppm
Fragment mass tolerance: - 0.5 Da
Max missed cleavages: 2
SAINT analysis
Exclusion of contaminants
Proteins with AvgP≥0.5
High confidence list of USP14-interacting partners
Functional validation

Supplemental Figure Legends

Supplemental Figure 1 (Figure S1). Construction of p-ES-NTAP-Puro vector. Related to Figure 2.

(A) The plasmid map of pCeMM-NTAP(GS)-Gw-Puro (p-ES-NTAP-Puro) is represented. Details of vector construction are described in the Materials and methods.

(B) Expression of p-ES-NTAP-Puro-USP14 in SH-SY5Y cells was verified by immunostaining against USP14 (red). Nuclei were stained with Hoechst dye (blue). Scale bar- 100 μm. Right panel- expression of the p-ES-NTAP-Puro-USP14 was verified by immunoblotting with USP14 antibody. The arrowhead marks the overexpressed NTAP-USP14 protein migrating at ~80 kDa, showing similar expression level as an endogenous USP14 (at ~55 kDa) in both conditions. No band at ~80 kDa is seen in SH-SY5Y cells expressing p-ES-NTAP-Puro vector only.

Supplemental Figure 2 (Figure S2). The workflow depicting the affinity purification and bioinformatic analysis of USP14 interacting partners. Related to Figure 2.

Retroviral infection compatible vector, pES-NTAP-Puro (USP14-NTAP-Puro) was utilized to infect SH-SY5Y cells and generate stably expressing clones upon puromycin selection. Cytoplasmic extracts were subjected to tandem affinity purification using dual affinity tags followed by FASP and tryptic digestion. Peptides were analyzed by tandem mass spectrometry and the results processed using Mascot and SAINT software. Contaminants were excluded based on the AvgP threshold resulting in a high confidence list of USP14-interacting partners (Supplemental Table 1). The identified interaction was further validated in Co-IP and functional experiments.

Supplemental Table 1: SAINT analysis of USP14 interacting partners in pES-NTAP-Puro-USP14 stably expressing SHSYSY-5Y cells recovered by TAP-MS. Related to Figure 2.

Bait	Prey	PreyGene	Spec	SpecSum	AvgSpec	NumReplicates	ctrlCounts	AvgP	MaxP	TopoAvgP	TopoMaxP	SaintScore	logOddsScore	FoldChange	BFDR	maxSpec	PreyGeneID	PreyGeneName	Project_Frequency	Shared_Frequency	BioGrid
USP14	HSP7C_HUMAN	HSPA8	2|4	6	3	2	0|0	0,99	1	1	1	1	6,02	30	0	4	3312	HSPA8	76,92	100	novel
USP14	IGHG2_HUMAN	IGHG2	3|3	6	3	2	0|0	1	1	1	1	1	5,41	30	0	3	3501	IGHG2	92,31	100	TAP contaminant
USP14	PRS4_HUMAN	PSMC1	10|16	26	13	2	0|0	1	1	1	1	1	38,9	130	0	16	5700	PSMC1		100	reported
USP14	PRS7_HUMAN	PSMC2	7|11	18	9	2	0|0	1	1	1	1	1	31,4	90	0	11	5701	PSMC2	23,08	100	reported
USP14	PRS6A_HUMAN	PSMC3	4|11	15	7,5	2	0|0	1	1	1	1	1	25,77	75	0	11	5702	PSMC3	15,38	100	reported
USP14	PRS8_HUMAN	PSMC5	5|6	11	5,5	2	0|0	1	1	1	1	1	29,21	55	0	6	5705	PSMC5	15,38	100	reported
USP14	PSMD1_HUMAN	PSMD1	4|14	18	9	2	0|0	1	1	1	1	1	24,72	90	0	14	5707	PSMD1	15,38	100	reported
USP14	PSMD2_HUMAN	PSMD2	9|16	25	12,5	2	0|0	1	1	1	1	1	35,95	125	0	16	5708	PSMD2	15,38	100	reported
USP14	PSMD3_HUMAN	PSMD3	8|12	20	10	2	0|0	1	1	1	1	1	35,09	100	0	12	5709	PSMD3		100	reported
USP14	PSMD4_HUMAN	PSMD4	3|5	8	4	2	0|0	1	1	1	1	1	23,33	40	0	5	5710	PSMD4		100	reported
USP14	HORN_HUMAN	HRNR	8|4	12	6	2	0|3	0,84	0,96	0,69	0,9	0,84	-0,07	4	0	8	388697	HRNR	84,62	100	statistical contaminant
USP14	ADRM1_HUMAN	ADRM1	1|5	6	3	2	0|0	0,5	1	0,5	1	0,5	15,24	30	0,12	5	11047	ADRM1		100	reported
USP14	PSA1_HUMAN	PSMA1	0|2	2	1	2	0|0	0,49	0,99	0,5	1	0,5	3,59	10	0,28	2	5682	PSMA1		100	novel
USP14	PSA2_HUMAN	PSMA2	1|4	5	2,5	2	0|0	0,5	1	0,5	1	0,5	13,48	25	0,17	4	5683	PSMA2	7,69	100	reported
USP14	PSA3_HUMAN	PSMA3	1|4	5	2,5	2	0|0	0,5	1	0,5	1	0,5	16,29	25	0,17	4	5684	PSMA3		100	reported
USP14	PSA5_HUMAN	PSMA5	0|3	3	1,5	2	0|0	0,5	1	0,5	1	0,5	5,7	15	0,2	3	5686	PSMA5	15,38	100	reported
USP14	PSA6_HUMAN	PSMA6	0|3	3	1,5	2	0|0	0,5	1	0,5	1	0,5	8,51	15	0,2	3	5687	PSMA6		100	reported
USP14	PSA7_HUMAN	PSMA7	0|6	6	3	2	0|0	0,5	1	0,5	1	0,5	6,4	30	0,09	6	5688	PSMA7		100	novel
USP14	PSB1_HUMAN	PSMB1	0|2	2	1	2	0|0	0,49	0,99	0,5	1	0,5	5	10	0,28	2	5689	PSMB1		100	reported
USP14	PSB5_HUMAN	PSMB5	0|8	8	4	2	0|0	0,5	1	0,5	1	0,5	9,92	40	0,02	8	5693	PSMB5		100	reported
USP14	PSB6_HUMAN	PSMB6	0|3	3	1,5	2	0|0	0,5	1	0,5	1	0,5	7,11	15	0,2	3	5694	PSMB6		100	novel
USP14	PSB7_HUMAN	PSMB7	0|3	3	1,5	2	0|0	0,5	1	0,5	1	0,5	7,81	15	0,2	3	5695	PSMB7		100	novel
USP14	PRS6B_HUMAN	PSMC4	0|5	5	2,5	2	0|0	0,5	1	0,5	1	0,5	9,92	25	0,12	5	5704	PSMC4	23,08	100	reported
USP14	PRS10_HUMAN	PSMC6	1|8	9	4,5	2	0|0	0,5	1	0,5	1	0,5	16,64	45	0,02	8	5706	PSMC6		100	reported
USP14	PSD11_HUMAN	PSMD11	2|1	3	1,5	2	0|0	0,49	0,99	0,5	1	0,5	18,05	15	0,28	2	5717	PSMD11		100	reported
USP14	PSD12_HUMAN	PSMD12	0|3	3	1,5	2	0|0	0,5	1	0,5	1	0,5	5	15	0,2	3	5718	PSMD12	15,38	100	reported
USP14	PSMD5_HUMAN	PSMD5	2|1	3	1,5	2	0|0	0,49	0,99	0,5	1	0,5	13,13	15	0,28	2	5711	PSMD5		100	novel
USP14	PSMD8_HUMAN	PSMD8	0|2	2	1	2	0|0	0,49	0,99	0,5	1	0,5	2,89	10	0,28	2	5714	PSMD8		100	novel
USP14	RS27A_HUMAN	RPS27A	0|3	3	1,5	2	0|0	0,5	1	0,5	1	0,5	-0,97	15	0,2	3	6233	RPS27A	92,31	100	statistical contaminant

Supplement Table Legend

Supplemental Table 1. List of interacting partners in USP14 overexpressing neuroblastoma cells. Related to Figure 2.

Tandem affinity analyses of USP14 interacting proteins were done as described in Transparent Methods section. Peptides obtained were analyzed using Mascot and SAINT software. Contaminants were excluded based on the AvgP threshold resulting in a high confidence list of USP14-interacting partners. Several proteasome interactors of USP14 have been reported, whilst the binding to HSPA8/HSC70 was previously unrecognized.

Transparent Methods

Cell culture and transfections

SH-SY5Y human and Neuro2A mouse neuroblastoma cells were cultured in Dulbecco's Modified Eagle Medium (DMEM) (Lonza) supplemented with 10% fetal bovine serum (Gibco), 7.5% NaHCO3, 100 mM NA-glutamine (Gibco) and 100 mM penicillin-streptomycin (Gibco) at 37°C in 5% CO_2. Striatal cell lines (kind gift from Prof. Tönis Timmusk, Tallin University of Technology, Estonia) derived from mice expressing different huntingtin (Htt) genotypes and immortalized with a temperature sensitive large T antigen were used as previously described (Kannike et al., 2014). Control cells expressed 7-polyglutamine (7Q) repeats while the mutant cells expressed 109-polyglutamine (109Q) repeats. Cells were cultured in DMEM supplemented with 10 % fetal bovine serum (Gibco), 7.5% NaHCO3, 100 mM NA-glutamine (Gibco) and 100 mM penicillin-streptomycin (Gibco) at 33°C in 5% CO_2.

Primary neuron cultures were obtained from brain cortices of embryonic E17-old rat pups, and cultured as described (Do et al., 2013). Briefly, the cortices were enzymatically dissociated by trypsin and further processed using DNase I (Roche). The solution was then centrifuged and the pellet resuspended in fresh Neurobasal solution (Gibco). The appropriate number of cells were plated onto cell culture dishes coated with poly-L-ornithine (Sigma) and cultured in Neurobasal (Gibco) medium supplemented with 50x B27 (Gibco), 25 mM glutamine (Gibco) and 100 mM penicillin-streptomycin (Gibco) at 37°C in 5% CO_2. Half of the medium was replaced every two days and cells were incubated for 8 days before experiments.

Different compounds were added to the cells, including 20 μM MG132 (Calbiochem), 0.5 μM bortezomib (Calbiochem) or 5 μM Lactacystin (Sigma) for 5-6 h to inhibit the proteasome. To inhibit autophagy, 200 nM bafilomycin A1 (Sigma) or 50 μM chloroquine (Sigma) were added for 5 h and to block the activity of HSC70, 25 or 50 μM VER-155008 (Tocris Biosciences) was added for 24 h. In some experiments, 2.5 μg/ml tunicamycin (Sigma) was added for 6 h to induce the unfolded protein response (UPR). Linear Polyethylenimine 25.000 (PEI) (Polysciences, Inc.) was used for transient transfection of neurons based on the manufacturer's instructions. PEI was prepared at a stock concentration of 1 mg/ml. DNA and PEI were combined at a ratio of 1:3 for complexing. Following 24 - 48 h of transfection, different treatments were applied as above.

Cell viability assay

Cell viability was assayed essentially as described previously (Hyrskyluoto et al., 2013). In brief, striatal cells expressing 7Q or 109Q Htt protein were treated with 25 μM or 50 μM VER-155008 for 24 h and cell death was measured by utilizing tetrazolium dye 3-(4,5-dimethylthiazol-2-yl)-2,5-

diphenyltetrazolium bromide (MTT, Sigma) substrate added to cells for 2 h. The insoluble formazan substrate was then reconstituted in a solvent of 0.1 M HCl-isopropanol and incubated for 30 min. with gentle agitation. Absorbance was measured at 560 nm and the value reflected the relative number of surviving cells following each treatment.

Expression vectors cDNAs and transfection

Wild type human pRK-FLAG-USP14 (Flag-WT-USP14) and mutant pRK-FLAG-USP14 C114A plasmids were a kind gift from Dr Yihong Ye (Wang et al., 2006). XBP1 (Myc-DDK-tagged)-Human X-box binding protein 1 (XBP1), transcript variant 1 (hereafter referred to as XBP1u) was obtained from Origene. pcDNA5/FRT/TO-GFP-HSPA8 (GFP-WT-HSC70), Flag-HA-GFP and Flag-HA-USP14 were obtained from Addgene. eGFP-WT-USP14 (GFP-WT-USP14) was generated by amplifying USP14 cDNA from pRK-FLAG-WT-USP14 and subcloning it into eGFPC1 vector. pDestEGFP-GABARAP (EGFP-GABARAP) plasmid was a kind gift from Dr. Nikolai Engedal (University of Oslo, Norway). The point mutation of WT-USP14 to W58A-USP14 was made using the QuickChange lightning site-directed mutagenesis kit (Stratagene) following the manufacturer's instructions.

pCeMM-NTAP(GS)-Gw-Puro cloning strategy

The details of pCeMM-CTAP(GS)-Gw-Puro (pES-CTAP) vector preparation were previously described (Scifo et al., 2013). In the first step, a fragment containing the IRES sequence and the puromycin ORF was amplified from pES-CTAP via PCR using the following primers: 5'-gttattttccaccatattgccg (5'-IRES_puro) and 5'-tcctcc<u>accggtacgcgt</u>caggcaccgggcttgcg (IRES_puro-3'; AgeI and MluI sites are underlined). The PCR fragment was then digested with AvrII (singular site in IRES) and AgeI (introduced by the PCR primer). This fragment was then ligated into the AvrII-BspEI site of the vector pCeMM-NTAP(GS)Gw (Burckstummer et al., 2006), thus replacing IRES-GFP by IRES-Puro casette from pES-CTAP vector. To achieve it, IRES-GFP was first removed from pCeMM-NTAP-GS-Gw by digesting the vector with AvrII (singular site in IRES) and Kpn2I (isoschizomer of BspEI, partial digest) thus isolating the BspEI (nt 1348) – AvrII vector band (size 7.4 kb). Potential clones were sequence verified using the following primers: 5'-gttattttccaccatattgccg (5'-IRES_puro) and 5'-caccgagctgcaagaactc (ML_Seq_1). The sequence and map of the pCeMM-NTAP(GS)-Gw-Puro vector are provided in the supplemental material.

Full length USP14 (OCAAo5051F0231D) sequence verified entry clone in pENTR221 vector, purchased from Source Biosource (<u>OCAAo5051F0231D</u>) was shuttled into pES-NTAP-Puro, for TAP-MS experiments, as described (Scifo et al., 2013). Recombination of DNA fragments was

performed using the LR clonase reaction (Life Technologies Europe BV, Espoo, Finland) and analyzed with BsrGI restriction enzyme.

Construct for shRNA against USP14

SHC002 Non-Mammalian (scramble shRNA) Negative control and constructs against human USP14 were purchased from TRC1 library in a backbone of pLKO.1 vector (Sigma). Five shRNA constructs were tested for efficient USP14 knockdown (KD) by immunoblotting for USP14 and the best constructs were then chosen for generation of SH-SY5Y USP14 KD cells. These constructs were TRCN0000007425 (USP14 shRNA1) and TRCN0000007428 (USP14 shRNA2).

Generation of SH-SY5Y human neuroblastoma cells with knockdown of USP14

Lentivirus particles expressing shRNA constructs were generated at the Biomedicum Functional Genomics Unit, University of Helsinki, Finland. SH-SY5Y cells were seeded into 6-well plates and transduced with lentiviral particles containing shRNA the following day. Following 48 h of virus infection, the antibiotic selection was performed by changing medium with fresh DMEM containing 1 µg/ml puromycin (Gibco, Life technologies). The shRNA constructs exhibiting the best USP14 KD efficiency were further chosen for expansion, referred to as USP14 shRNA1 and USP14 shRNA2 cell clones. SH-SY5Y cells transduced with scramble shRNA expressing viruses were used as a control. Selection pressure with puromycin was maintained during propagation and the medium was changed every 3 days with fresh DMEM containing puromycin.

TAP purification

Monolayer cells were harvested from three 150 mm plates of USP14-NTAP-Puro or NTAP-Puro infected SH-SY5Y cells, grown to 80% confluency (1×10^8 cells). Preparation of cytoplasmic extract from the cells was performed as previously described (Scifo et al., 2013), while the TAP purification procedure followed by FASP preparation prior to MS analysis as in (Scifo et al., 2015a). The Lys-C and trypsin peptide digests were processed on Zip-Tip C18 reversed phase (Merck Millipore) according to manufacturer protocol. Peptide digests were resuspended in 1% TFA and sonicated in a water bath for 1 min. The peptide mixture was applied onto a C-18 reverse phase pre-column (nanoACQUITY Symmetry® C18, Waters) using 0.1% TFA as mobile phase and then separated on a nano-UPLC C-18 column (nanoACQUITY BEH C18, Waters) with an 0.05% formic acid in a gradient of acetonitrile (0–35% ACN in 182 min), at a flow rate of 250 nl/min, and analyzed on Q Exactive™Hybrid Quadrupole-Orbitrap (Thermo Scientific), as described (Scifo et al., 2015a). MS/MS peak lists or spectral data were searched with the Mascot Daemon interface (version 2.4.0;

Matrix Science, Uni. of Helsinki) against the Swiss-Prot 2018_05 database (20350 sequences), with taxonomy set to Homo sapiens. Carbamidomethyl-Cys, met oxidation and N/Q residues deamidation were used as fixed and variable modifications, respectively. Mass tolerance of the precursor ions was set to 20 ppm, and of MS/MS fragment ions to 0.5 Da. The peptide charges were set to 1-3, and 2 tryptic mis-cleavages were allowed. SAINT analysis was performed as previously described (Scifo et al., 2013), except that two biological replicates were used for the bait (USP14) and negative control (empty pES-NTAP-Puro vector). Protein hits that passed the threshold of an AvgP ≥0.5 were considered as true USP14 interactors, after exclusion of an empty pES-NTAP-Puro vector contaminants (Scifo et al., 2013; Scifo et al., 2015a, b), statistical contaminants (www.crapome.org) and checking for those matching the list of previously identified USP14 interacting partners (see compendium in BioGRID 3.5 database; Biogrid/homo-sapiens/usp14).

Immunoprecipitation

Cells were lysed in a modified RIPA lysis buffer containing 50 mM Tris-HCl pH 7.7, 150 mM NaCl, 1% NP-40, and 0.5% sodium deoxycholate for 30 min. on ice. Following the lysis, the tubes were rotated for 15-30 min. at 4°C and centrifuged at 10,000g for 10 min. at 4°C. The supernatant was collected, and protein concentration was measured using the BCA protein assay kit (Pierce, Thermo Fisher Scientific). Equal amounts of protein lysates were taken and precleared using 20 µl of prewashed Protein A/G agarose beads (Sigma) for one hour at 4°C. Pre-cleared lysate was incubated with the Anti-Flag M2 (Sigma) or Anti-USP14 (Sigma) overnight in a rotor at 4°C. The following day, BSA blocked agarose beads were added to the overnight antibody conjugated lysate mixture and was left to rotate at 4°C for 2-3 h. The antibody complexed beads were centrifuged at 9000xg for 1 min. at 4°C and washed with the lysis buffer 3-4 times on a rotator at 4°C, 5 min. each. Immunoprecipitated proteins were eluted by adding 35 µl of 2x denaturing Laemmli buffer and heated at 95°C for 5 min. The heat-denatured samples were centrifuged for 3 min. at 10.000xg and the supernatant was collected. The 35 µl supernatant was loaded to PAGE and the immunoprecipitated complexes were analyzed using Western blot for detecting the immunoprecipitated protein and its interacting partners. 40 µg of lysate was used as the input control.

Immunoblotting

Cells were washed twice with ice-cold PBS and lysed in RIPA buffer (150 mM NaCl, 1% Triton-X-100, 0.5% sodium deoxycholate, 1% SDS, 50 mM Tris-HCl, pH 7.4) supplemented with protease inhibitors (Roche) and phosphatase inhibitor (Phosphostop, Roche). Protein concentration measurements were performed with the BCA protein assay kit (Pierce, Thermo Fisher Scientific),

and equal amounts of protein were loaded to PAGE and blotted onto nitrocellulose membrane filters (Amersham Biosciences, Helsinki, Finland). The membranes were incubated for 1h in 5% skimmed milk or 5% bovine serum albumin, in TBS-T (50 mM Tris-HCl pH 7.5, 150 mM NaCl, 0.1% Tween 20) and then with the primary antibodies overnight at 4°C with gentle agitation. Primary antibodies used were as follows: anti-USP14 (1:500, Abgent, AP2142a); anti-USP14 (1:1000, Sigma, J6111-6D6); anti-HSC70 (1:2000, SantaCruz Biotechnology, sc7298); anti-XBP1 (detects both XBP1s running at 56 kDa and XBP1u, at 29 kDa as indicated in respective IBs and figure legends), 1:2000, Cell signaling technologies, D2C1F); anti-Actin (1:10000,Sigma, A2066); Anti-GFP (1:2000, Sigma, 11814460001); anti-Flag (1:2000, Sigma); Anti-pIRE1α (phosphor S724; 1:2500, Abcam, ab48187), Anti-IRE1α (1:2500, Abcam, ab37073); Anti-PSMD2 (1:1000, Thermo Fisher Scientific); anti-GABARAP (E14JE) (1:2000, CST, 13733). Following washes, the membranes were incubated with horseradish peroxidase-conjugated secondary antibodies (1:2500, Jackson Immunoresearch Laboratories) at room temperature for 1 h with gentle agitation. Protein signals were detected using enhanced chemiluminescence substrate (Pierce, Thermo Fisher Scientific). Immunoblots were quantified with ImageJ (NIH) quantification software.

Immunocytochemistry

SH-SY5Y cells or Striatal neuronal cells plated on coverslips were fixed using 4% paraformaldehyde at RT for 10 min. Fixed cells were permeabilized with 0.1% Triton-X-100 containing phosphate buffered saline (PBS-T) and blocked with 5% bovine serum albumin (Sigma) diluted in PBS-T for 1 h. The cells were incubated in XBP1u antibody (1:500; SAB2102720, Sigma) diluted in 5% BSA containing PBS-T overnight at 4°C. The coverslips were washed in PBS-T and incubated with fluorophore conjugated Alexa Fluor® 488 or 594 secondary antibody diluted in 5% BSA containing PBS-T (1:600, Invitrogen) for 2 h in dark at room temperature. Subsequently, the coverslips were washed in PBS-T and nuclei stained with Hoechst 33342 (Thermo Fisher Scientific, 62249). The coverslips were mounted onto glass slides with Mowiwol (Calbiochem) containing DABCO gel mounting media. The cells were imaged using Zeiss Axioplan2 imaging universal light microscope.

Live cell imaging for EGFP-GABARAP positive autophagic structures

Striatal neuronal cells transfected with EGFP-GABARAP in combination with empty vector or Flag-W58A-USP14 were imaged using the EVOS FL cell imaging system (Thermo Fisher Scientific) with a 40X objective. Imaging of GABARAP positive autophagosome at a higher resolution was performed using a Nikon Eclipse Ti-E inverted widefield microscope with full environmental chamber, Hamamatsu Orca Flash 4.0 V2 B&W camera for fluorescence and Lumencor Spectra X

light engine (Biomedicum imagine unit, Medicum, University of Helsinki). Briefly, striatal neurons were plated on µ-Slide ibiTreat polymer bottom plates (80826, ibidi, Germany) and transfected with EGFP-GABARAP in combination with empty vector or Flag-W58A-USP14. Following the treatment with VER-155008 (25µM, 24 h) or DMSO, cells were imaged with a 100X Plan Apo VC objective (Numerical aperture, 1.40) and LED-FITC-A filter. Images were acquired using NIS-Elements advanced research with 6D image acquisition module software from Nikon.
Each experiment contained images from several fields of view. Acquired images were analyzed by ImageJ particle analysis.

Analysis for XBP1u ALIS and EGFP-GABARAP positive structures

XBP1u ALIS and EGFP-GABARAP autophagic structures were considered as particles and analyzed using ImageJ ComDet v.0.4.1 plugin. Briefly, the region of interest (ROI) was defined around the cell boundary. The plugin was applied to the defined ROI to obtain the number of particles and their respective integrated intensities. To negate the cell size dependent differences in the number of particles, average integrated intensity/particle was obtained and used as a measure of changes in XBP1u ALIS or EGFP-GABARAP signal intensities between samples.

Deubiquitination activity assay

The assay was performed as described earlier with a few modifications (Borodovsky et al., 2002). Neuro2A cells overexpressing Flag-WT-USP14, Flag-C114A-USP14, and Flag-W58A-USP14 were lysed in 50 mM Tris (pH 7.4), 250 mM sucrose, 5 mM $MgCl_2$, 1mM DTT and 1mM ATP for 1h at 4°C. 50 µg of lysates was then incubated with 3 mM ubiquitin vinyl methyl ester (HA tag; Enzo Life Science) for 3 h at 37°C. The samples were then boiled 95°C for 5 min in denaturing Laemmli buffer and analyzed by immunoblotting with anti-Flag antibodies.

RNA isolation and Quantitative PCR

RNA was extracted from control 7Q and mutant 109Q expressing striatal cells using the RNeasy mini kit (Qiagen). cDNA was synthesized with SuperScript VILO (Invitrogen, Thermo Fisher Scientific Scientific) following the manufacturer's instructions. LightCycler 480 SYBR Green I MASTER (Roche Applied Science) was utilized to perform real time quantitative PCR on a LightCycler 480 (Roche Applied Science) with a 96-well block as described previously (Pham et al., 2016; Pham et al., 2019). PCR conditions were as follows: Initial incubation at 95 °C for 15 min, followed by 40 cycles at 95 °C for 15 s, 63 °C for 20 s and 72 °C for 10 s. Each sample was analyzed in triplicates and from three independent experiments and normalized to glyceraldehyde-3-phosphate

dehydrogenase (GAPDH) using the ΔΔCt (threshold cycle) method. The amplified product was checked by melting curve analysis spanning the temperature range from 65 °C to 95 °C with a ramping rate of 0.03 °C/s. The following primer sequences were used: USP14, forward, 5'GGCGAACAAGGGCAGTATC3', and reverse, 5'TCTGTTGCAGGACTCTCATCA3';
GAPDH, forward, 5'GGGTTCCTATAAATACGGACTGC3', and reverse, 5'CCATTTTGTCTACGGGACGA3'.

Statistical analysis

Statistical comparison was performed using Student's t-test or one-way/two-way ANOVA, depending on the experimental design. p value, $p < 0.05$ was considered as statistically significant. Statistical analysis and graph design were performed using GraphPad PRISM software.

Supplemental References

Borodovsky, A., Ovaa, H., Kolli, N., Gan-Erdene, T., Wilkinson, K.D., Ploegh, H.L., and Kessler, B.M. (2002). Chemistry-based functional proteomics reveals novel members of the deubiquitinating enzyme family. Chem. Biol. *9*, 1149-1159.

Burckstummer, T., Bennett, K.L., Preradovic, A., Schutze, G., Hantschel, O., Superti-Furga, G., and Bauch, A. (2006). An efficient tandem affinity purification procedure for interaction proteomics in mammalian cells. Nat. Methods *3*, 1013-1019.

Do, H.T., Bruelle, C., Tselykh, T., Jalonen, P., Korhonen, L., and Lindholm, D. (2013). Reciprocal regulation of very low density lipoprotein receptors (VLDLRs) in neurons by brain-derived neurotrophic factor (BDNF) and Reelin: involvement of the E3 ligase Mylip/Idol. J. Biol. Chem. *288*, 29613-29620.

Hyrskyluoto, A., Pulli, I., Tornqvist, K., Ho, T.H., Korhonen, L., and Lindholm, D. (2013). Sigma-1 receptor agonist PRE084 is protective against mutant huntingtin-induced cell degeneration: involvement of calpastatin and the NF-kappaB pathway. Cell Death Dis. *4*, e646.

Kannike, K., Sepp, M., Zuccato, C., Cattaneo, E., and Timmusk, T. (2014). Forkhead transcription factor FOXO3a levels are increased in Huntington disease because of overactivated positive autofeedback loop. J. Biol. Chem. *289*, 32845-32857.

Pham, D.D., Do, H.T., Bruelle, C., Kukkonen, J.P., Eriksson, O., Mogollon, I., Korhonen, L.T., Arumae, U., and Lindholm, D. (2016). p75 Neurotrophin Receptor Signaling Activates Sterol Regulatory Element-binding Protein-2 in Hepatocyte Cells via p38 Mitogen-activated Protein Kinase and Caspase-3. J. Biol. Chem. *291*, 10747-10758.

Pham, D.D., Bruelle, C., Thi Do, H., Pajanoja, C., Jin, C., Srinivasan, V., Olkkonen, V.M., Eriksson, O., Jauhiainen, M., Lalowski, M.*, et al.* (2019). Caspase-2 and p75 neurotrophin receptor (p75NTR) are involved in the regulation of SREBP and lipid genes in hepatocyte cells. Cell Death Dis. *10*, 537.

Scifo, E., Szwajda, A., Debski, J., Uusi-Rauva, K., Kesti, T., Dadlez, M., Gingras, A.C., Tyynela, J., Baumann, M.H., Jalanko, A.*, et al.* (2013). Drafting the CLN3 protein interactome in SH-SY5Y human neuroblastoma cells: a label-free quantitative proteomics approach. J. Proteome Res. *12*, 2101-2115.

Scifo, E., Szwajda, A., Soliymani, R., Pezzini, F., Bianchi, M., Dapkunas, A., Debski, J., Uusi-Rauva, K., Dadlez, M., Gingras, A.C.*, et al.* (2015a). Proteomic analysis of the palmitoyl protein thioesterase 1 interactome in SH-SY5Y human neuroblastoma cells. J. Proteomics *123*, 42-53.

Scifo, E., Szwajda, A., Soliymani, R., Pezzini, F., Bianchi, M., Dapkunas, A., Debski, J., Uusi-Rauva, K., Dadlez, M., Gingras, A.C.*, et al.* (2015b). Quantitative analysis of PPT1 interactome in human neuroblastoma cells. Data Brief *4*, 207-216.

Wang, Q., Li, L., and Ye, Y. (2006). Regulation of retrotranslocation by p97-associated deubiquitinating enzyme ataxin-3. J. Cell Biol. *174*, 963-971.